FEDERAL UNIVERSITY OF SÃO CARLOS
CENTER OF SCIENCE AND TECHNOLOGIES FOR SUSTAINABILITY
POSTGRADUATE PROGRAM IN PLANNING AND USE OF RENEWABLE RESOURCES

Tamaki Kugimiya

Tension in Hardwoods:
Radial Property Distribution and the Role of Hygrothermal Recovery

Sorocaba
2025

FEDERAL UNIVERSITY OF SÃO CARLOS
CENTER OF SCIENCE AND TECHNOLOGIES FOR SUSTAINABILITY
POSTGRADUATE PROGRAM IN PLANNING AND USE OF RENEWABLE RESOURCES

Tamaki Kugimiya

Tension in Hardwoods:
Radial Property Distribution and the Role of Hygrothermal Recovery

Dissertation presented to Postgraduate Program in Planning and Use of Renewable Resources to obtain the Master's degree in Planning and Use of Renewable Resources from the Federal University of São Carlos. Area of concentration: Sustainable production.

Supervisor: Prof. Dr. Fabio M. Yamaji
Co-supervisor: Prof. Dr. Hiroyuki Yammoto

Sorocaba
2025

Kugimiya, Tamaki

Tension in hardwoods: radial property distribution and the role of hygrothermal recovery / Tamaki Kugimiya -- 2025.
72f.

Dissertação (Mestrado) - Universidade Federal de São Carlos, campus Sorocaba, Sorocaba
Orientador (a): Fabio Minoru Yamaji
Banca Examinadora: Fabio Minoru Yamaji, Gabriela Tami Nakashima, Felipe Augusto Santiago Hansted
Bibliografia

1. Hygrothermal recovery. 2. Tension wood. 3. Growth stress. I. Kugimiya, Tamaki. II. Título.

Ficha catalográfica desenvolvida pela Secretaria Geral de Informática (SIn)

DADOS FORNECIDOS PELO AUTOR

Bibliotecário responsável: Maria Aparecida de Lourdes Mariano - CRB/8 6979

UNIVERSIDADE FEDERAL DE SÃO CARLOS

Centro de Ciências e Tecnologias Para a Sustentabilidade
Programa de Pós-Graduação em Planejamento e Uso de Recursos Renováveis

Folha de Aprovação

Defesa de Dissertação de Mestrado do candidato Tamaki Kugimiya, realizada em 04/11/2025.

Comissão Julgadora:

Prof. Dr. Fábio Minoru Yamaji (UFSCar)

Profa. Dra. Gabriela Tami Nakashima (CBA)

Prof. Dr. Felipe Augusto Santiago Hansted (Anhanguera)

O Relatório de Defesa assinado pelos membros da Comissão Julgadora encontra-se arquivado junto ao Programa de Pós-Graduação em Planejamento e Uso de Recursos Renováveis.

ACKNOWLEDGMENTS

I would like to express my sincere gratitude to my supervisors, Professor Hiroyuki Yamamoto and Professor Fabio M. Yamaji, for their guidance and support. I am also grateful to Associate Professor Masato Yoshida (Wood Physics Laboratory at Nagoya University), Dr. Hang Wan (Wood physics Laboratory at Nagoya University) and Associate Professor Miyuki Matsuo (Kyoto University), Dr. Naohisa Kameyama (Kameyama Construction) for their assistance. Regarding the calculation of *C.I.*, I appreciate the help of Mr. Akiyoshi Nishiyama and Mr. Shunsuke Otsuki, as well as Ms. Fuyuno Yamada of the Forest Resources Management Laboratory at Nagoya University. I am grateful to all the seniors, peers, and juniors in the Wood Physics Laboratory at Nagoya University. I would like to thank the Isotope Research Center of Nagoya University (Chikusa-ku, Nagoya, Japan) for their cooperation in the XRD measurements.

ABSTRACT

KUGIMIYA, Tamaki. The mechanism of hygrothermal recovery in tension wood. 2025. Dissertation (Master in Planning and Use of Renewable Resources) - Federal University of São Carlos, Sorocaba, 2025.

In the current era of progressing global warming, the value of forests and wood has been increasing. Trees develop growth stress as a survival strategy to grow tall; however, these stresses become obstacles when humans utilize wood. The elastic component of growth stress is released during felling and sawing, while the viscoelastic component is released during boiling. The latter is referred to as hygrothermal recovery (HTR). Although various studies on HTR have been conducted, its detailed behavior remains unclear. This study aims to understand the radial distribution of wood properties and the role of HTR in hardwood containing tension wood. In Chapter 3, HTR was examined from the bark to the pith together with the G-layer proportion, crystallinity index (C.I.), microfibril angle (MFA), and drying strain. In Chapter 4, HTR was evaluated under various treatment temperatures and durations, along with drying mass change, crystallite size (L), and d-spacing for comparison. In Chapter 3, the results showed that HTR alone exhibited dependence on the distance from the pith and contributed to the release of the viscoelastic component of growth stress. In Chapter 4, in the tangential (T) direction, viscoelastic release of compressive growth stress was confirmed by detecting the expansion of d-spacing between cellulose molecular chains. In the longitudinal (L) direction, it was confirmed that the viscoelastic release of tensile growth stress likely occurs at a more macroscopic level—such as contractive relaxation of pre-stretched cellulose microfibrils (CMFs)—rather than through a decrease in the d-spacing of cellulose crystallites along the molecular axis. For future studies, analysis using FTIR and small-angle scattering are desirable to elucidate the behavior of the matrix and CMFs during HTR.

Keywords: hygrothermal recovery, tension wood, growth stress, hardwood

Table of contents

Chapter 1: General Introduction

1.1 Benefits of utilization of wood

In recent years, as global warming has intensified, the value of forests and wood has increased. According to The State of the World's Forests 2024, forests and trees offer cost-effective solutions to the climate and biodiversity crises. Forest and Forestry White Paper (2025) states that the use of wood contributes to the prevention of global warming from the following three perspectives:

① carbon storage,
② substitution for energy-intensive resources, and
③ substitution for fossil fuels.

Regarding ①, Figure 1 shows the global carbon cycle, in which the carbon stock in forests is included under "vegetation". Forests play a role in carbon stock. Figure 2 shows forest carbon stock in biomass. Until around 2010, this stock showed a decreasing trend due to forest degradation and forest fires, but by 2020, it had shifted to an increasing trend. The carbon (CO_2) absorbed by trees can be stored semi-permanently when wood is used as wood engineered products.

Figure 1 The global carbon cycle

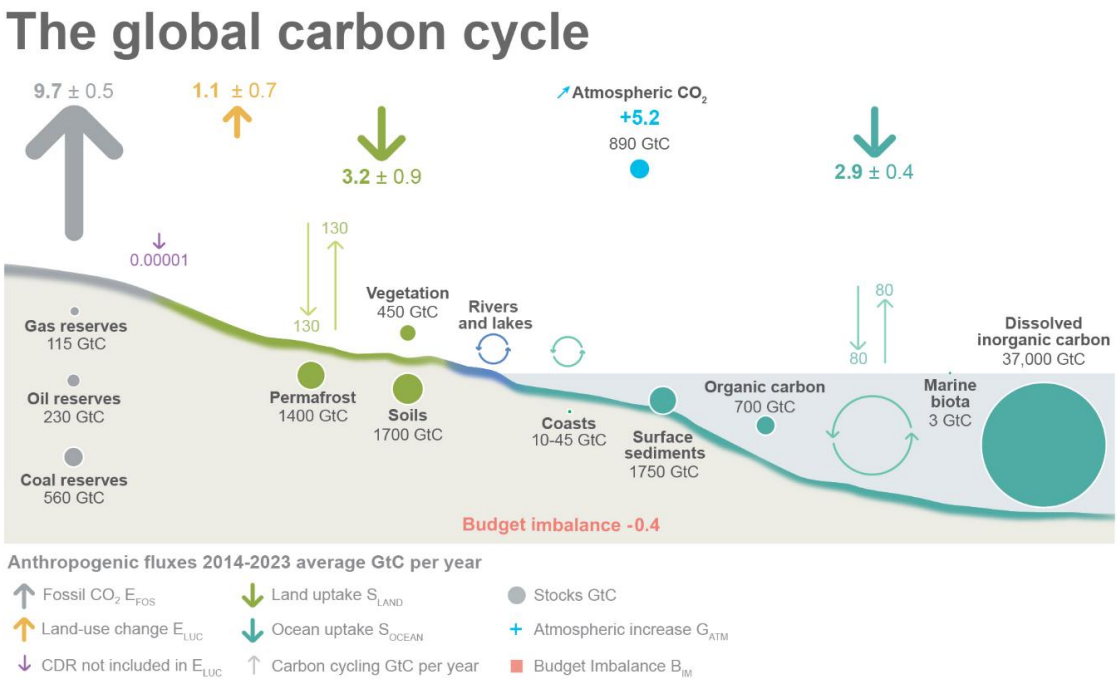

Source: Global Carbon Budget (2024)

Figure 2 -Forest Carbon stock in biomass

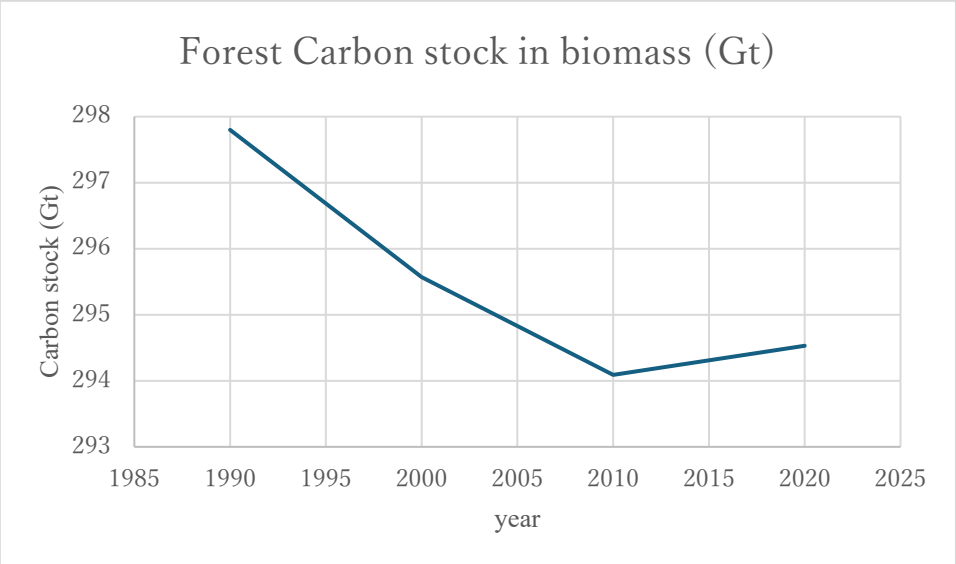

Source: Global Forest Resources Assessment (2020)

Regarding ②, substituting wood for other materials, such as steel and aluminum, reduces fossil fuel consumption during material production. Table 1 shows the amount of fossil fuel consumed in the production of each material. It can be seen that air-dried timber and kiln-dried timber consume significantly fewer fossil fuels compared to other materials.

Table 1 - Fossil fuel consumption during material production

	MJ/kg	MJ/m^3
Air-dried timber	1.5	750
Kiln-dried timber	2.8	1,390
Plywood	12.0	6,000
Particleboard	20.0	10,000
Steel	35.0	266,000
Aluminum	435.0	1,100,000
Concrete	2.0	4,800

Source: Arima (2003)

While the use of wood helps reduce fossil fuel consumption, it is also important to consider substituting fossil fuels with wood when reusing timber reclaimed from buildings. (MINISTRY OF AGRICULTURE, FORESTRY AND FISHERIES, 2025).

Regarding ③, fossil fuels originate from ancient carbon that is hundreds of millions of years old; therefore, using fossil fuels adds new carbon to the atmosphere. In contrast, wood originates from atmospheric carbon, so the use of wood can be considered carbon neutral (Friedlingstein et al., 2024).

As explained above, wood utilization contributes to storage carbon, reducing the use of fossil fuels and substitution for fossil fuels. But in utilizing wood, growth stress and reaction wood—introduced below—can sometimes pose challenges even though they were necessary for tree to live (Gril *et al*. 2017).

1.2 Growth stress

In order to support vertical development, trees induce surface growth stress near the bark, characterized by tensile forces. With maturation, these stresses progressively accumulate, forming residual growth stress (Figure 3).

Figure 3 - Surface growth stress and residual growth stress

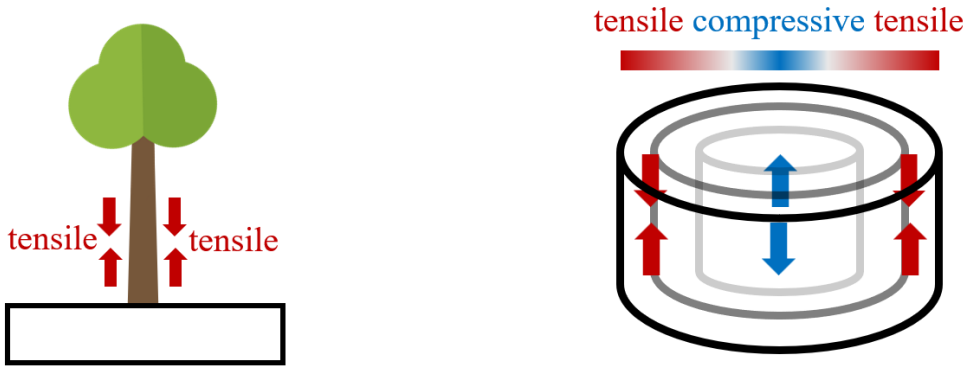

Source: Author's own

Although residual growth stress is necessary for tree to gain advantage in the struggle for survival, it causes processing defect when it was used by human. The distribution of residual growth stress causes end-splitting in logs by releasing residual growth stress during cutting and boiling (Castéra *et al*., 1994; Jullien *et al*., 2003; Hernández *et al*., 2014; Nistal *et al*., 2020; Rozas *et al*., 2021). It causes yield loss of up to 30% (FAO, 1966) (Figure 4). Although waste wood is used for biofuel (Nakano *et al*. 2024), deformations caused by releasing of growth stress limit wood utilization. The releasing of growth stress by steaming or boiling is called hygrothermal recovery (HTR) (Kubler, 1987). HTR is explained in chapter 2.3 in detail.

Figure 4 - End-splitting in log

Source: Kameyama (2025), Doctoral dissertation

1.3 Reaction wood

Reaction wood refers to the specialized tissue formed by trees growing on slopes in order to exhibit negative gravitropism. Conifers form compression wood (CW) on the lower side of the inclined stem to push the trunk upward, while hardwoods form tension wood (TW) on the upper side to pull the trunk upward (Figure 5).

Figure 5 – Reaction wood of softwood (left) and hardwood (right)

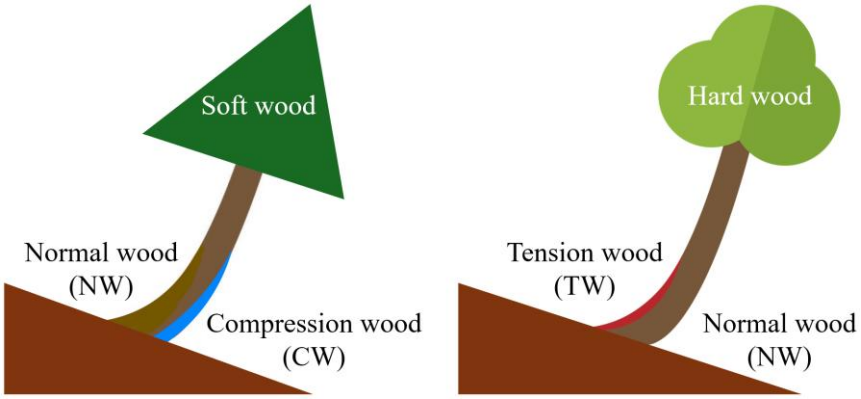

Source: Author’s own

Together, Compression wood (CW) and Tension wood (TW) are collectively called reaction wood. CW has a higher proportion of matrix material and a larger cellulose microfibril angle (CMA) compared to normal wood (NW). In contrast, TW contains a higher proportion of cellulose and has a smaller CMA than NW (Yamamoto and Okuyama, 1993; Yamamoto and Okuyama, 1994). Anatomically, CW tracheids tend to have a more rounded shape than those in NW (Timell, 1986; Donaldson and Singh, 2013) (Figure 6).

Figure 6 - Anatomical features of Compression wood (CW) (left) and Normal wood (NW) (right)

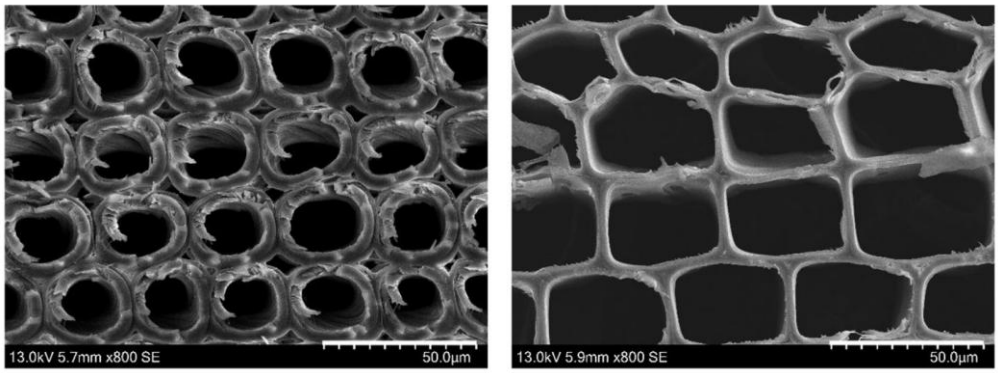

Source: Peng *et al.* (2019)

While TW often develops a gelatinous layer (G-layer) on the innermost surface of the xylem fibers (Onaka, 1949) (Figure 7).

Figure 7 - Anatomical features of Tension wood (TW) (left) and Normal wood (NW) (right)

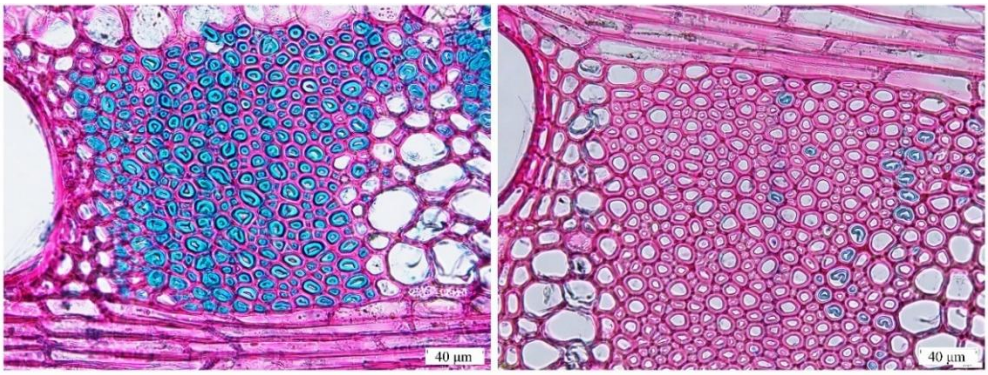

Source: Author's own

Although reaction wood is important for trees to resist the force of gravity, the distribution of reaction wood in a tree causes deformation when we process wood. CW and TW accumulate compressive and tensile stress, respectively. These stresses are released during cutting and boiling. As a result, wood shows deformation (Kitahara *et al*., 1986; Okuyama *et al*., 1994).

1.4 Hardwood utilization

Hardwood is used for furniture and construction (Figure 8 (a), (b)), but it is less utilized than softwood because it is difficult to process. Hardwood often shows complex shapes caused by growth stress (Figure 8 (c)). However, it has a beautiful grain (Figure 8 (d)). For example, in Japan, keyaki (*Zelkova serrata* Makino) is used for traditional structures such as shrines and temples. Therefore, understanding the properties of hardwood is important for expanding its utilization.

Figure 8 - Hardwood utilization

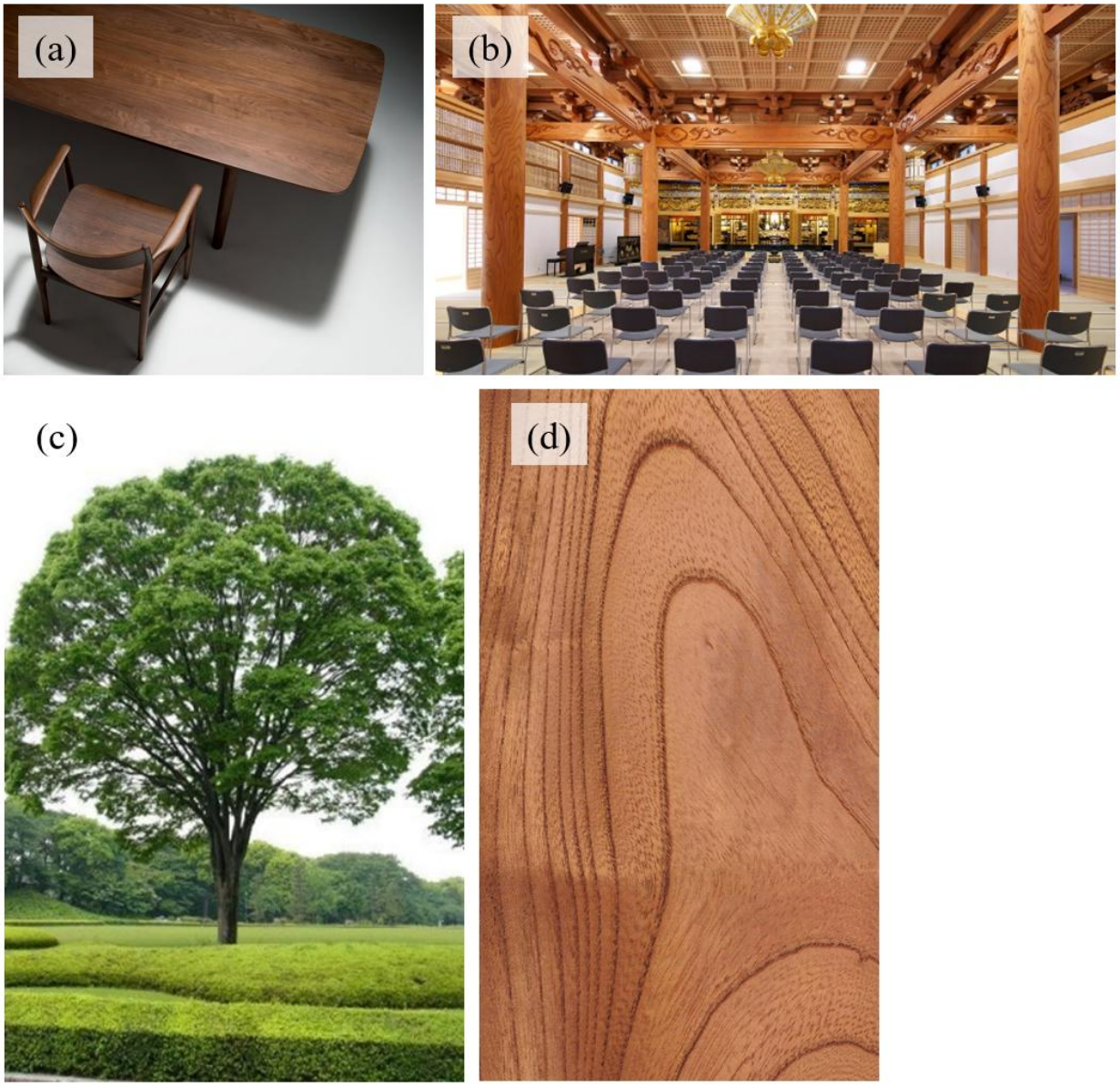

Source: (a) CondeHouse; (b) Kameyama (2025), Doctoral dissertation;
(c) & (d) https://wood-museum.net/keyaki.php

1.5 Purpose of present study

During processing, complex deformations are induced by superposition of distributions of residual growth stress with stress in reaction wood and releasing of those. Understanding the mechanism of releasing stress is necessary for sustainable use of wood. Especially, the releasing of stresses during boiling is referred as hygrothermal recovery (HTR) (Kubler, 1987).

The aim of this study is to understand the behavior of hygrothermal recovery (HTR) by using hardwood (*Zelkova serrata* Makino) containing tension wood. In chapter 3, the radial distributions of HTR strain in a disk were measured with radial distributions of the G-layer proportion, crystallinity index (*C.I.*), microfibril angle (*MFA*), drying strain to clarify the variations in the behaviors of wood. In chapter 4, HTR strains were measured with drying mass change, crystallite size (*L*), and *d-spacing* under various treatment temperatures and durations.

Ultimately, this fundamental study provides a mechanistic and quantifiable foundation necessary for developing effective industrial pre-treatments and Non-Destructive Testing (NDT) criteria. And understanding the mechanism of HTR contributes to the identification of optimal uses for trees and their local regions, and the control of growth stress and tree shape.

References

ARIMA, T. Wood science for housing – Considering wooden architecture. **University of Tokyo Press**, 2003.

CASTÉRA, P.; NEPVEU, G.; MAHÉ, F.; VALENTIN, G. A study on growth stresses, tension wood distribution and other related wood defects in poplar (Populus euramericana cv 1214): end splits, specific gravity and pulp yield. **Ann For Sci**, v. 51, p. 301–313, 1994.

DONALDSON, L. A.; SINGH, A. P. Structure and formation of compression wood. In: FROMM, J. (ed.) *Cellular aspects of wood formation*. Plant Cell Monographs. **Springer, Heidelberg**, 2013. p. 225–256.

FOOD AND AGRICULTURE ORGANIZATION OF THE UNITED NATIONS (FAO). Unasylva, Vol. 20 (1-2): An International Review of Forestry and Forest Industries – Wood: World Trends and Prospects. Rome: **FAO**, 1966.

FOOD AND AGRICULTURE ORGANIZATION OF THE UNITED NATIONS (FAO). Global Forest Resources Assessment 2020. **FAOSTAT**, 2020.

FOOD AND AGRICULTURE ORGANIZATION OF THE UNITED NATIONS (FAO). The State of the World's Forests 2024. **The State of the World's Forests 2024**, 2024.

FRIEDLINGSTEIN, P.; O'SULLIVAN, M.; JONES, M. W.; *et al*. Global Carbon Budget 2024, 2024.

GRIL, J.; JULLIEN, D.; BARDET, S.; YAMAMOTO, H. Tree growth stress and related problems. **J Wood Sci**, 63:411–432, 2017.

INTERNATIONAL ENERGY AGENCY (IEA). Carbon neutrality – Bioenergy. Available at: https://www.ieabioenergy.com/iea-publications/faq/woodybiomass/carbon-neutrality/#:~:text=Within%20the%20biospheric%20carbon%20cycle%2C%20bioenergy%20can%20be,as%20the%20plants%20regrow%2C%20i.e.%20if%20sustainably%20produced. Accessed: 28 Oct. 2025.

HERNÁNDEZ, M.; ZADERENKO, C.; MONTEOLIVA, S. Tensiones de crecimiento y propiedades físicas de la madera de Eucalyptus dunnii implantado en Argentina. **Maderas, Cienc Tecnol**, v. 16,

p. 373–384, 2014.

JAPAN SOCIETY OF CIVIL ENGINEERS (JSCE). Introduction to wood use in civil engineering – Toward environmental contributions in civil engineering. **Wood Engineering Special Committee, JSCE**, 2011.

JULLIEN, D.; GRIL, J. Modelling crack propagation due to growth stress release in round wood. **J Phys IV France**, v. 105, p. 265–272, 2003.

KITAHARA, R.; TSUTSUMI, J.; MATSUO, T. Wood Deformations Due to Growth Stress Release. **Bulletin of the Utsunomiya University Forests**, 22:49–60, 1986.

KÜBLER, H. Growth stresses in trees and related wood properties. **For Products Abs**, v. 10, p. 61–119, 1987.

MINISTRY OF AGRICULTURE, FORESTRY AND FISHERIES (MAFF). Forest and Forestry White Paper, 2025. **Government of Japan**, Tokyo, 2025.

NAKANO, K.; KOIDE M.; YAMADA Y.; *et al*. Environmental impacts of structural lumber production in Japan. **Journal of Wood Science**, v. 70, p. 4, 2024.

NISTAL FRANÇA FJ, FILGUEIRA AMORIM FRANÇA TS, VIDAURRE GB. Effect of growth stress and interlocked grain on splitting of seven different hybrid clones of Eucalyptus grandis × Eucalyptus urophylla wood. **Holzforschung**, 74:917–926, 2020.

OKUYAMA, T.; YAMAMOTO, H.; YOSHIDA, M. *et al*. Growth stresses in tension wood: role of microfibrils and lignification. **Ann For Sci**, 51:291–300, 1994.

ONAKA, F.; Studies on compression- and tension-wood. **Wood Research**, 1:1–88, 1949.

PENG, H.; SALMÉN, L.; STEVANIC, J. S.; LU, J. Structural organization of the cell wall polymers in compression wood as revealed by FTIR microspectroscopy. **Planta**, v. 250, p. 163–171, 2019.

TIMELL, T. E. Compression wood in gymnosperms. **Springer**, Berlin, 1986.

TOBA, K.; YAMAMOTO, H.; YOSHIDA, M. Micromechanical detection of growth stress in wood

cell wall by wide-angle X-ray diffraction (WAX). **Holzforschung**, v. 67, p. 315–323, 2013.

ROZAS, C.; VASQUEZ, M.; VEGA, P.; *et al*. Investigating Storage Time to Minimize End-Splitting in Eucalyptus Nitens Logs. **WFS**, 55:228–241, 2024.

Chapter 2: Literature review

2.1 Wood structure

The wood cell wall consists of approximately 50% cellulose, 20–30% hemicellulose, and 20–30% lignin (PETTERSEN, 1984). Within the wood cell wall, cellulose molecules bundle together to form cellulose microfibrils (CMFs), and hemicellulose and lignin are located in the spaces between these CMFs, creating a composite structure (Figure 9). Since cellulose is crystalline while hemicellulose and lignin are amorphous, hemicellulose and lignin are collectively referred to as the matrix.

Figure 9 - CMFs within the wood cell wall and its crystalline structure

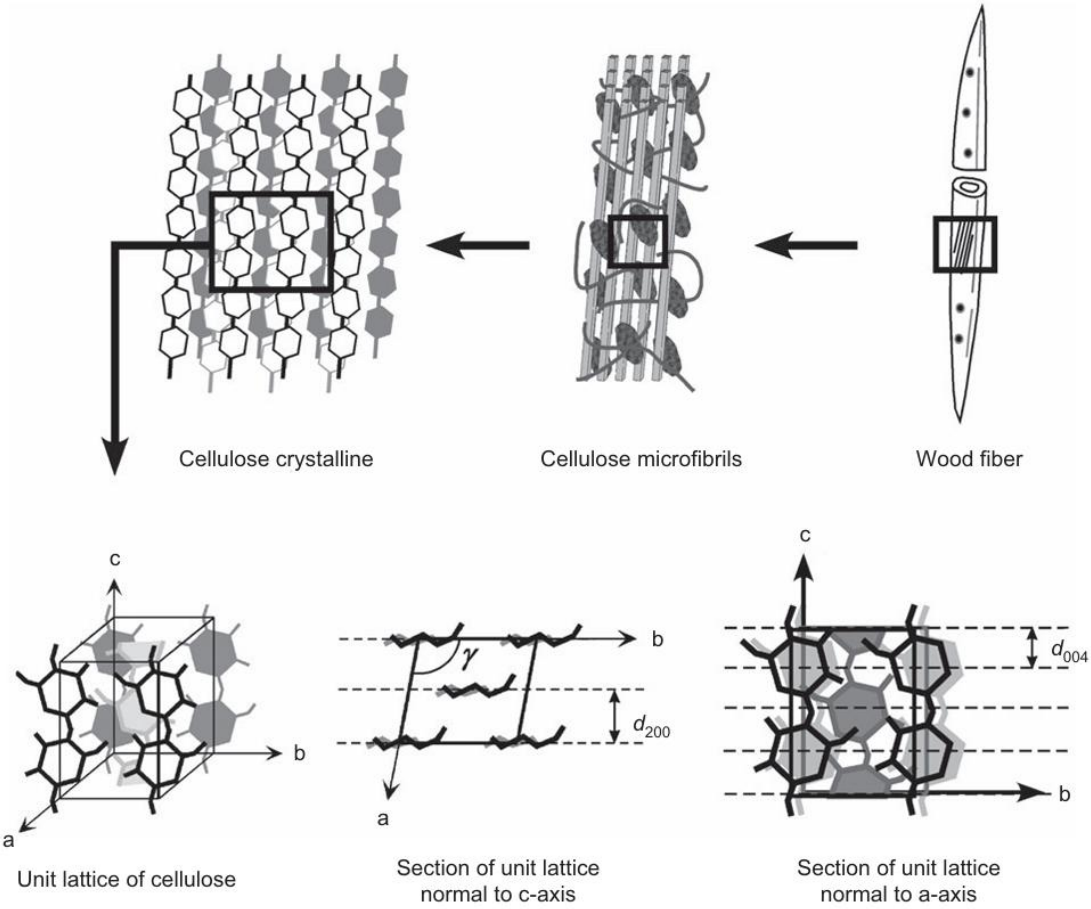

Source: Toba *et al.* (2013)

2.2 Reaction wood and Growth stress

Figure 10 shows the trend in the number of publications on “reaction wood” or “tension wood” or “compression wood” in Web of Science. Research on this topic has been conducted for nearly 100 years, and the number of publications has shown an increasing trend since around 2000.

Figure 10- Number of publications and citations with the terms “reaction wood” and “tension wood” or “compression wood” searched in the Web of Science.

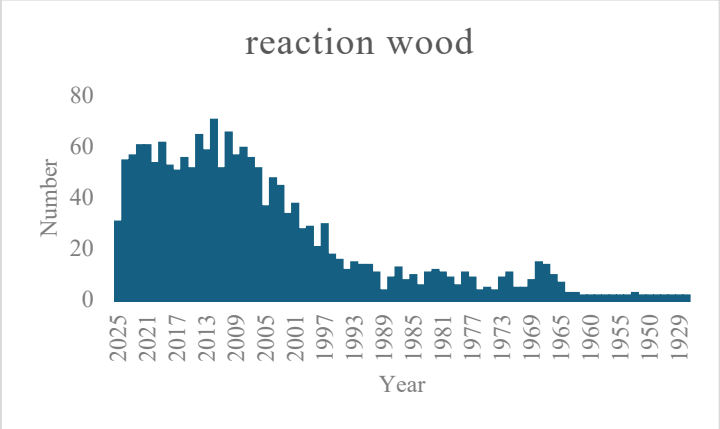

Source: Author’s own

Figure 11 shows the main categories and their proportions, displaying only those categories that account for more than 5% of the total categories. This data shows that reaction wood is of interest not only in forestry but also in materials science as well as plant science.

Figure 11 - The main research categories involving the terms “reaction wood” and “tension wood” or “compression wood” and their proportion (%) searched in the Web of Science.

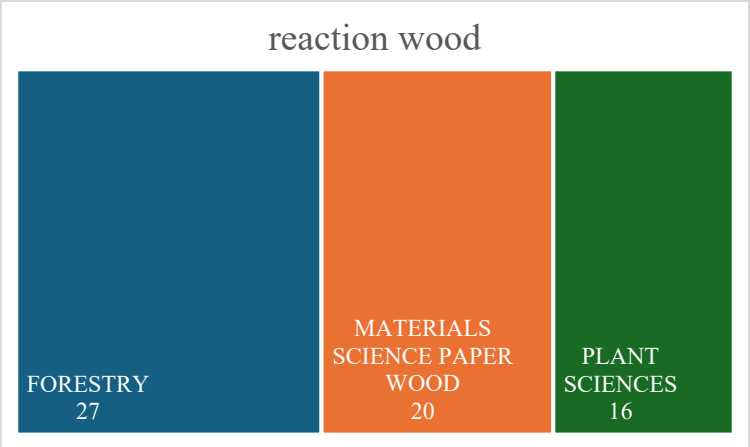

Source: Author’s own

Figure 12 shows the main research countries of reaction wood. Japan's papers account 10% in total papers of reaction wood. In Japan, after the domestic wood self-sufficiency rate reached its lowest point in 2002, both the self-sufficiency rate and the supply of domestically produced timber increased (Figure 13). This is because Russia raised export tariffs on softwood logs between 2007 and 2008, which reduced the import volume of northern logs and made it necessary to use domestic timber more efficiently (JAPAN FORESTRY AND FORESTRY EDUCATION CENTER, 2025) In addition, technological innovations have made it possible to produce plywood from small-diameter logs such as thinnings, which has also contributed to the increase in the wood self-sufficiency rate (MINISTRY OF AGRICULTURE, FORESTRY AND FISHERIES, 2025). So, it can be considered that the renewed promotion of wood utilization has occurred, leading to an increase in research on processing defects. Additionally, compared to the search results for *growth stress*, the proportion of Plant Science is higher. This is likely because, in addition to applied research for wood utilization, anatomical and genetic fundamental research is also actively conducted.

Figure 12 - The main research countries involving the terms "reaction wood" or "tension wood" or "compression wood" and their proportion (%) searched in the Web of Science.

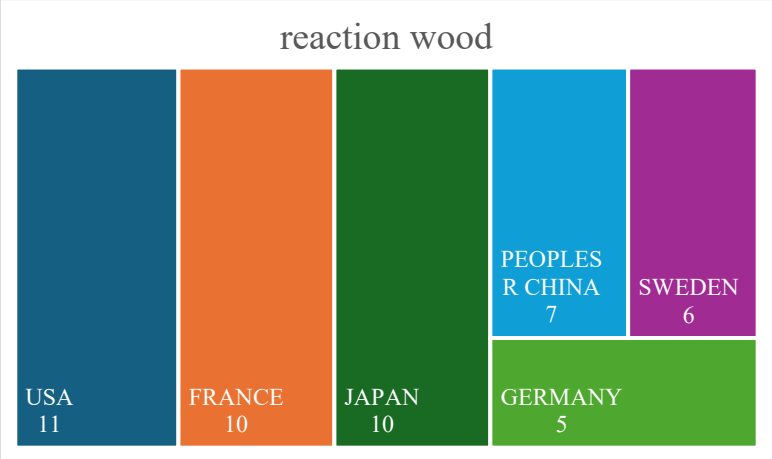

Source: Author's own

Figure 13 Trends in wood demand in Japan.

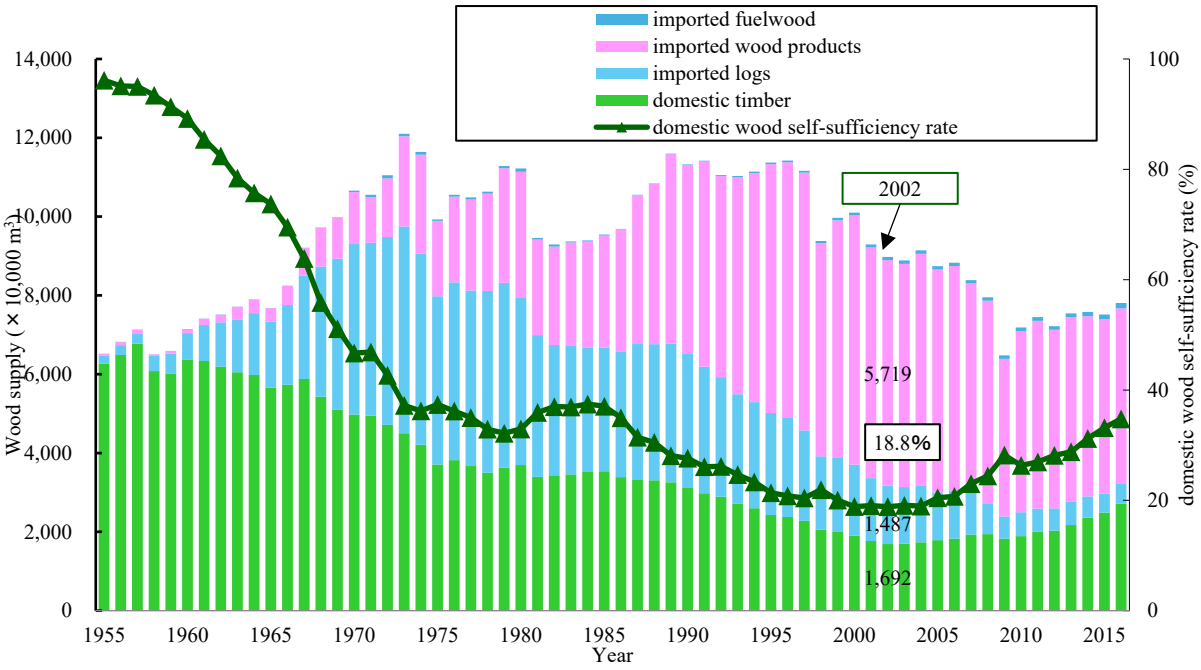

Source: FOREST AGENCY OF JAPAN (2024)

Figure 14 shows the trend in the number of publications on “growth stress” and “wood” in Web of Science. It indicates that research on this topic has been ongoing for over 40 years. The irregular trend in the number of publications is likely because there are few researchers working on growth stress, and the number is influenced by their experimental and writing schedules. In addition, number of publications of growth stress is less than those of reaction wood. It is considered to be due to the bias in the main research categories of growth stress compared with those of reaction wood (Figure 12 & Figure 15).

Figure 14- Number of publications and citations with the terms “growth stress” and “wood” searched in the Web of Science.

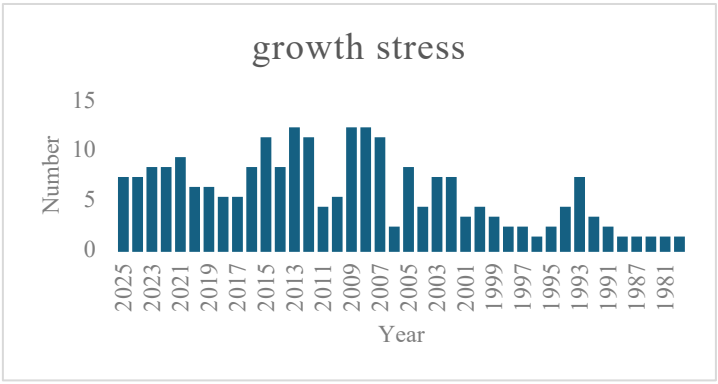

Source: Author’s own

Figure 15 shows the main categories and their proportions, displaying only those categories that account for more than 5% of the total categories. This data also shows that growth stress is of interest not only in forestry but also in materials science as well as plant science.

Figure 15 - The main research categories involving the terms “growth stress” and “wood” and their proportion (%) searched in the Web of Science.

Source: Author’s own

Mechanisms of Growth Stress Generation in terms of reaction wood and growth stress

There are mainly three hypotheses regarding the mechanism of growth stress generation in wood formation. The first hypothesis is the “Lignin Swelling Hypothesis” proposed by Watanabe (1967) and Boyd (1972). According to this hypothesis, the matrix containing lignin is constrained by the rigid cellulose, causing expansion of the matrix in the direction perpendicular to the orientation of cellulose. This hypothesis explains the tangential surface growth stress.

The second hypothesis is the “Cellulose Tension Hypothesis” proposed by Bamber (1978), which developed the idea of Wardrop (1965). This hypothesis suggests that the cellulose microfibrils (CMFs) themselves generate tensile stress, explaining the longitudinal surface growth stress.

The third hypothesis is the “Unified Hypothesis” by Okuyama (1993). In this model, the first hypothesis is applied to regions with a large microfibril angle (*MFA*), and the second hypothesis is applied to regions with a small *MFA*.

Figure 16 – Unified hypothesis

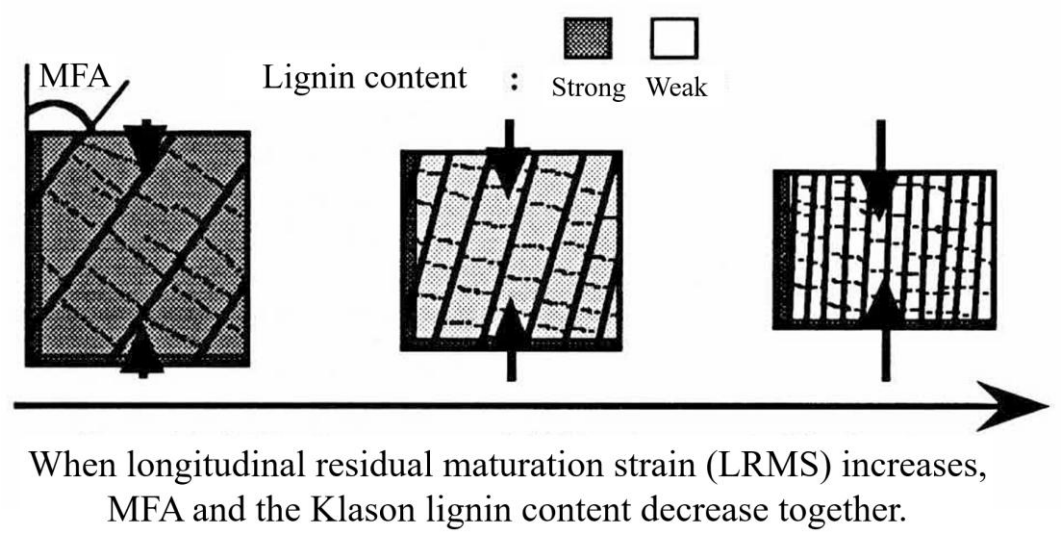

Sorce: Author’s own based on Baillères *et al.*1995

Reaction wood is useful as a comparative reference to normal wood (NW) in terms of chemical composition and structure. Therefore, it is often used when examining hypotheses regarding the mechanism of growth stress generation.

Okuyama (1994) used tension wood (TW), which has a smaller microfibril angle (*MFA*) and a higher cellulose content than NW, to investigate the correlation between longitudinal tensile surface growth stress and physical properties (G-layer cross-sectional area, *MFA*, cellulose content, crystallinity, lignin content). This study demonstrated the effectiveness of the unified hypothesis, particularly in cases where the *MFA* is small. Subsequently, Okuyama (1998) used compression wood (CW), which has a larger *MFA* and higher lignin content than NW, to examine the correlation between longitudinal compressive surface growth stress and lignin content, demonstrating the effectiveness of the unified hypothesis for regions with a large *MFA*.

Since then, research supporting the unified hypothesis has continued through measurements of G-layer proportion, *MFA*, chemical composition, and comparisons with mechanical models (Baillères *et al.*, 1995; Guitard *et al.*, 1999; Yoshida *et al.*, 2002; Yamamoto *et al.*, 2004; Yamamoto, 2005; Ruelle *et al.*, 2006; Hang *et al.*, 2007; Fang *et al.*, 2008a,b; Hirohashi *et al.*, 2012).

However, some studies, such as Clair (2006), have compared stress levels with G-layer occurrence and suggested that the G-layer is not the primary factor in the formation of wood with high tensile stress. This indicates that continued data collection is necessary.

Detailed studies on the unified hypothesis—specifically, how and what triggers matrix swelling and CMF contraction—have progressed as follows:

Yoshida (2003) investigated the generation of tangential surface growth stress and showed that tangential strain increases at night, resulting from changes in moisture content and the volume changes of differentiating cells. Furthermore, TW contains more moisture than NW and expands more during the night. Almeras (2006) studied the generation of longitudinal surface growth stress and suggested that the development of longitudinal growth stress in TW and CW is not directly related to changes in turgor pressure or diurnal strain. For longitudinal tensile growth stress, xyloglucan has been suggested to play a role in generating the tensile stress and standing the tensile stress created within the G-layer as a main non-cellulose component in G-layer. (Mellerowicz *et al.*, 2008; Baba *et al.*, 2009).

From these findings, it was suggested that the generation of growth stress perpendicular to the *MFA* is influenced by matrix swelling due to increased moisture content, whereas the generation of growth stress parallel to the *MFA* is not affected by moisture content and may be influenced by xyloglucan.
Other studies have suggested that lignin deposition and xylem formation are affected by gravitational stimuli (Yoshida *et al.*, 2005) and light stimuli (Matsuzaki *et al.*, 2007; Almeras *et al.*, 2009). Yoshida (2005) showed that gravitational stimuli influence the distribution of lignin deposition.
Subsequent research on the mechanism of growth stress generation has advanced by incorporating the concept of hygrothermal recovery (HTR); this will be discussed in Section 2.2 HTR.

Wood Utilization and Growth Stress

The economic penalty associated with growth stress is significant. During processing, growth stress can cause warping and cracking, reducing yield (FAO, 1966). For this reason, some studies have used growth stress measurements to predict end-splitting in logs (Castéra *et al.*, 1994; Jullien *et al.*, 2003; Hernández *et al.*, 2014; Nistal *et al.*, 2020; Rozas *et al.*, 2021). Additionally, research has been conducted on traits for selecting individuals with low growth stress and predicting the magnitude of growth stress (Santos *et al.*, 2004; Trugilho *et al.*, 2008; Biechele *et al.*, 2009; Watanabe *et al.*, 2012; Solirvano *et al.*, 2012; Jullien *et al.*, 2013). Some studies have even explored reducing growth stress using herbicides (Cademartori *et al.*, 2015; Silva *et al.*, 2017).
However, growth stress can also be advantageous in wood utilization. For example, some studies have shown that high growth stress contributes to increased wind resistance (Zanuncio *et al.*, 2017).

2.3 HTR

When a tree is felled, the elastic component of growth stress is released immediately, while boiling releases the viscoelastic component, also known as the locked-in stress. The latter is referred to as hygrothermal recovery (HTR). The first mention of the relationship between HTR and growth stress is attributed to Koehler (1933) (at that time, the term HTR had not yet been defined).
Figure 17 shows the trend in the number of publications on “hygrothermal recovery” and “wood” in Web of Science, while Figure 18 shows the main categories and their proportions, displaying only those categories that account for more than 5% of the total categories.
The term Hygrothermal Recovery (HTR) was defined in a review by Kubler (1987), based on the study by Yokota and Tarkow (1962) (Chafe, 1992; Gril and Thibaut, 1994). Since the term was defined relatively recently, the number of publications is still limited, but research on this topic has been ongoing for over 30 years.

Figure 17 - Number of publications and citations with the terms “hygrothermal recovery” and “wood” searched in the Web of Science.

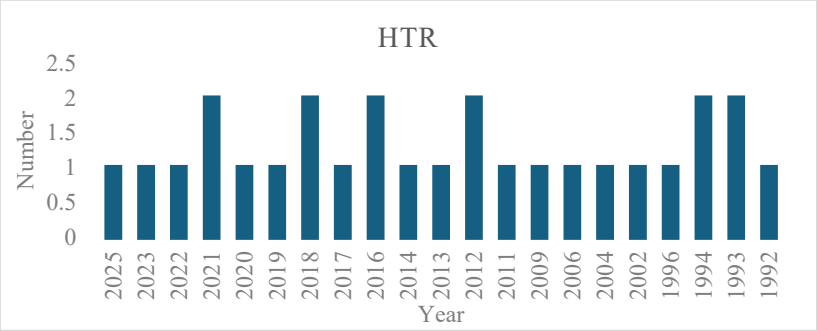

Source: Author’s own

Figure 18 - The main research categories involving the terms “hygrothermal recovery” and “wood” and their proportion searched in the Web of Science.

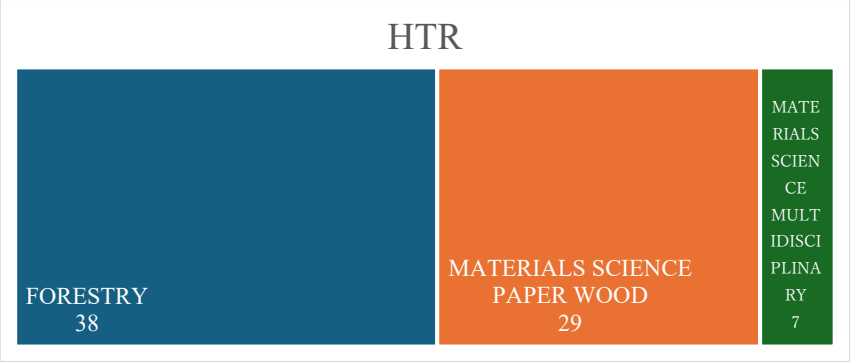

Source: Author’s own

Mechanisms of Growth Stress Generation in terms of HTR

In Section 2.1 *Growth Stress and Reaction Wood*, studies supporting the unified hypothesis were introduced based on measurements of G-layer proportion, *MFA*, chemical composition, and comparisons with mechanical models. In this section, we introduce studies that approached the elucidation of growth stress generation mechanisms by examining the relationship between HTR and growth stress.

To investigate the behavior of cellulose during HTR in detail, measurements of *d-spacing* were made using Wide-angle X-ray scattering (WAXS) before and after HTR have been conducted (Abe *et al.*, 2005, 2006 and 2007; Toba *et al.*, 2013). These studies suggest that growth stress is released through contraction of CMFs in the direction parallel to the *MFA* and expansion of the spacing between cellulose chains in the perpendicular direction, indicating matrix swelling.

To study matrix behavior in HTR in detail, HTR measurements have been performed under various temperature conditions below the cellulose softening point (Sujan *et al.*, 2016; Matsuo *et al.*, 2016; Chen *et al.*, 2019; Chen *et al.*, 2021; Yamamoto *et al.*, 2022; Matsuo *et al.*, 2023; Jing *et al.*, 2025). Since CW has a higher lignin content than NW and TW has a lower lignin content than NW, reaction wood has been used in these studies as well. These studies support the unified hypothesis while suggesting that lignin, in particular, may influence the release of growth stress within the matrix.

The release of growth stress is not only achieved through HTR but can also be induced by repeated wetting and drying or by dimethyl sulfoxide (DMSO) treatment (Tanaka *et al.*, 2014; Sujan *et al.*, 2018; Chen *et al.*, 2020). By altering the moisture content of the matrix through these treatments, volume changes in the matrix are induced, and behaviors similar to HTR are observed. These studies also demonstrate the usefulness of approaching the mechanism of growth stress generation from the perspective of HTR.

Wood Utilization and HTR

Understanding HTR behavior is also important from the perspective of wood utilization. HTR has both aspects that promote cracking and aspects that relieve residual stress (Kubler, 1959, 1987; Fonti *et al.*, 2002; Nogi *et al.*, 2003; Berard *et al.*, 2006; Kong *et al.*, 2017; Calihego *et al.*, 2021; Moya *et al.*, 2022). HTR has also been modeled (Gril *et al.*, 1994; Bardet *et al.*, 2012; Lancha *et al.*, 2021). These models are effective not only for predicting HTR behavior but also as models of tree growth.

References

ABE, K.; YAMAMOTO, H. Mechanical interaction between cellulose microfibril and matrix substance in wood cell wall determined by X-ray diffraction. **J Wood Sci**, v. 51, p. 334–338, 2005.

ABE, K.; YAMAMOTO, H. Change in mechanical interaction between cellulose microfibril and matrix substance in wood cell wall induced by hygrothermal treatment. **J Wood Sci**, 52:107–110, 2006.

ABE, K.; YAMAMOTO, H. The influences of boiling and drying treatments on the behaviors of tension wood with gelatinous layers in Zelkova serrata. **J Wood Sci**, v. 53, p. 5–10, 2007.

ALMÉRAS, T.; DERYCKE, M.; JAOUEN, G.; *et al*. Functional diversity in gravitropic reaction among tropical seedlings in relation to ecological and developmental traits. **Journal of Experimental Botany**, v. 60, p. 4397–4410, 2009.

ALMÉRAS, T.; YOSHIDA, M.; OKUYAMA, T. The generation of longitudinal maturation stress in wood is not dependent on diurnal changes in diameter of trunk. **J Wood Sci**, v. 52, p. 452–455, 2006.
BABA, K.; PARK, Y. W.; KAKU, T.; *et al*. Xyloglucan for generating tensile stress to bend tree stem. **Molecular Plant**, v. 2, p. 893–903, 2009.

BAILLÈRES, H.; CHANSON, B.; FOURNIER, M.; *et al*. Structure, composition chimique et retraits de maturation du bois chez les clones d'Eucalyptus. **Ann For Sci**, v. 52, p. 157–172, 1995.

BAMBER, R.K. The origin of growth stress, Contributed paper. **IUFRO Conference**, Philippines, pp. 7, 1978.

BARDET, S.; GRIL, J.; KOJIRO, K. Thermal strain of green Hinoki wood: separating the hygrothermal recovery and the reversible deformation. In: FRÉMOND, M.; MACERI, F. (eds.). **Mechanics, Models and Methods in Civil Engineering**. **Springer Berlin Heidelberg**, Berlin, Heidelberg, p. 157–162, 2012.

BERARD, P.; LAURENT, T.; DUMONCEAUD, O. Use of round wood of chestnut tree coppices: crack risk and effects of a hot oil bath treatment. **Holz Roh Werkst**, v. 64, p. 287–293, 2006.
BIECHELE, T.; NUTTO, L.; BECKER, G. Growth strain in Eucalyptus nitens at different stages of development. **Silva Fenn**, v. 43, p. 669–679, 2009.

BOYD, J. D. Tree growth stresses - Part V: evidence of an origin in differentiation and lignification. **Wood Science and Technology**, v. 6, p. 251–262, 1972.

CADEMARTORI, P. H. G. D.; GATTO, D. A.; STANGERLIN, D. M.; *et al*. Uso de herbicida na redução das tensões de crescimento na madeira serrada de Eucalyptus grandis. **Ciênc Florest**, v. 25, p. 801–808, 2015.

CASTÉRA, P.; NEPVEU, G.; MAHÉ, F.; VALENTIN, G. A study on growth stresses, tension wood distribution and other related wood defects in poplar (Populus euramericana cv 1214): end splits, specific gravity and pulp yield. **Ann For Sci**, v. 51, p. 301–313, 1994.

CHAFE, S. C. The effect of boiling time on the change in green wood volume in Eucalyptus regnans F. Muell. **Holzforschung**, v. 46, p. 463–446, 1992.

CHEN, S.; MATSUO-UEDA, M.; YOSHIDA, M.; YAMAMOTO, H. Changes in vibrational properties of compression wood in conifer due to hygrothermal treatment and their relationship with hygrothermal recovery strain. **J Mater Sci**, v. 54, p. 3069–3081, 2019.

CHEN, S.; MATSUO-UEDA, M.; YOSHIDA, M.; YAMAMOTO, H. Hygrothermal recovery behavior of cellulose-rich gelatinous layer in tension wood studied by viscoelastic vibration measurement. **Cellulose**, v. 28, p. 5793–5805, 2021.

CHEN, S.; MATSUO-UEDA, M.; YOSHIDA, M.; YAMAMOTO, H. Hygrothermal recovery of compression wood in relation to DMSO swelling and drying shrinkage. **Holzforschung**, v. 74, p. 789–797, 2020.

CLAIR, B.; ALMÉRAS, T.; YAMAMOTO, H.; *et al*. Mechanical behavior of cellulose microfibrils in tension wood, in relation with maturation stress generation. **Biophysical Journal**, v. 91, p. 1128–1135, 2006.

FANG, C.-H.; CLAIR, B.; GRIL, J.; LIU, S.-Q. Growth stresses are highly controlled by the amount of G-layer in poplar tension wood. **IAWA J**, v. 29, p. 237–246, 2008a.

FANG, C.-H.; GUIBAL, D.; CLAIR, B.; *et al*. Relationships between growth stress and wood properties in poplar I-69 (Populus deltoides Bartr. cv. “Lux” ex I-69/55). **Ann For Sci**, v. 65, p. 307–

307, 2008b.

FONTI, P.; MACCHIONI, N.; THIBAUT, B. Ring shake in chestnut (Castanea sativa Mill.): state of the art. **Ann For Sci**, v. 59, p. 129–140, 2002.

FOOD AND AGRICULTURE ORGANIZATION OF THE UNITED NATIONS (FAO). Unasylva, Vol. 20 (1-2): An International Review of Forestry and Forest Industries – Wood: World Trends and Prospects. Rome: **FAO**, 1966.

FOREST AGENCY OF JAPAN. R5 (2023) Wood Supply and Demand Table. Tokyo: **Forest Agency of Japan**, 2024.

FUKUSHIMA, K.; FUNADA, R.; SUGIYAMA, J.; TAKABE, K.; UMEZAWA, T.; YAMAMOTO, H. (Eds.). Secondary Xylem Formation - Introduction to Biomass Science (2nd ed.). **Kaiseisha Press**, 2011.

GRIL, J.; THIBAUT, B. Tree mechanics and wood mechanics: relating hygrothermal recovery of green wood to the maturation process. **Ann For Sci**, v. 51, p. 329–336, 1994.

GUITARD, D.; MASSE, H.; YAMAMOTO, H.; OKUYAMA, T. Growth stress generation: a new mechanical model of the dimensional change of wood cells during maturation. **J Wood Sci**, v. 45, p. 384–391, 1999.

HERNÁNDEZ, M.; ZADERENKO, C.; MONTEOLIVA, S. Tensiones de crecimiento y propiedades físicas de la madera de Eucalyptus dunnii implantado en Argentina. **Maderas, Cienc Tecnol**, v. 16, p. 373–384, 2014.

HIROHASHI, A.; KOJIMA, M.; YOSHIDA, M.; *et al*. Wood properties of 6 fast-growing Eucalyptus species grown in Japan. **Mokuzai Gakkaishi**, v. 58, p. 339–346, 2012.

JAPAN FORESTRY AND FORESTRY EDUCATION CENTER. *Wood supply and self-sufficiency rate in Japan.* [s.l.], 2025. Available at: https://www.shinrin-ringyou.com/data/mokuzai_kyoukyu.php. Accessed on: Nov. 5, 2025.

JING, Q.; YAMAMOTO, H.; YOSHIDA, M.; *et al*. The interrelation of microfibril angle and the lignified S2 layer on hygrothermal recovery in juvenile and mature compression wood of Cryptomeria

japonica and Chamaecyparis obtusa. **Wood Sci Technol**, v. 59, p. 77, 2025.

JULLIEN, D.; GRIL, J. Modelling crack propagation due to growth stress release in round wood. **J Phys IV France**, v. 105, p. 265–272, 2003.

JULLIEN, D.; WIDMANN, R.; LOUP, C.; THIBAUT, B. Relationship between tree morphology and growth stress in mature European beech stands. **Ann For Sci**, v. 70, p. 133–142, 2013.

KONG, L.; ZHAO, Z.; HE, Z.; YI, S. Effects of steaming treatment on crystallinity and glass transition temperature of Eucalyptuses grandis×E. urophylla. **Results in Physics**, v. 7, p. 914–919, 2017.

KUO-HUANG, L.-L.; CHEN, S.-S.; HUANG, Y.-S.; *et al*. Growth strains and related wood structures in the leaning trunks and branches of Trochodendron aralioides - a vessel-less dicotyledon. **IAWA J**, v. 28, p. 211–222, 2007.

LANCHA, JP.; COLIN, J.; ALMEID, A G. *et al*. A validated Distributed Activation Energy Model (DAEM) to predict the chemical degradation of biomass as a function of hydrothermal treatment conditions. **Bioresource Technology**, 341:125831, 2021.

MATSUO-UEDA, M.; YOSHIDA, M.; YAMAMOTO, H.; Analysis of hygrothermal recovery of tension wood induced by boiling at 50–80 °C. **Holzforschung**, 77:270–282, 2023.

MATSUZAKI, J.; MASUMORI, M.; TANGE, T. Phototropic bending of non-elongating and radially growing woody stems results from asymmetrical xylem formation. **Plant Cell & Environment**, 30:646–653, 2007.

MELLOWICZ, E. J.; IMMERZEEL, P.; HAYASHI, T. Xyloglucan: The Molecular Muscle of Trees. **Annals of Botany**, 102:659–665, 2008.

MOYA, R.; TENORIO, C. Reduction of effect of growth stress presence using endless screw during kiln drying and steaming and heating treatment in log before sawing. **WR**, 67:157–169, 2022.

NISTAL FRANÇA, F. J.; FILGUEIRA AMORIM FRANÇA, T. S.; VIDAURRE, G. B. Effect of growth stress and interlocked grain on splitting of seven different hybrid clones of *Eucalyptus grandis* × *Eucalyptus urophylla* wood. **Holzforschung**, 74:917–926, 2020.

NOGI, M.; YAMAMOTO, H.; OKUYAMA, T. Relaxation mechanism of residual stress inside logs by heat treatment: choosing the heating time and temperature. **J Wood Sci**, 49:0022–0028, 2003.

OKUYAMA, T. Growth Stress in Trees. **Mokuzai Gakkaishi**, v. 39, p. 747–756, 1993.

OKUYAMA, T.; TAKEDA, H.; YAMAMOTO, H.; YOSHIDA, M. Relation between growth stress and lignin concentration in the cell wall: Ultraviolet microscopic spectral analysis. **J Wood Sci**, 44:83–89, 1998.

OKUYAMA, T.; YAMAMOTO, H.; YOSHIDA, M. *et al*. Growth stresses in tension wood: role of microfibrils and lignification. **Ann For Sci**, 51:291–300, 1994.

PETTERSEN, R. C. The chemical composition of wood. In: ROWELL, R. M. (Ed.). *The Chemistry of Solid Wood.* Washington, D.C.: **American Chemical Society**, 1984. p. 57–126.

ROZAS, C.; VASQUEZ, M.; VEGA, P. *et al*. Investigating storage time to minimize end-splitting in *Eucalyptus nitens* logs. **WFS**, 55:228–241, 2024.

RUELLE, J.; CLAIR, B.; BEAUCHÊNE, J. *et al*. Tension wood and opposite wood in 21 tropical rain forest species 2. Comparison of some anatomical and ultrastructural criteria. **IAWA Journal**, 25:341–376, 2006.

SANTOS, P. E. T. D.; GERALDI, I. O.; GARCIA, J. N. Estimates of genetic parameters of wood traits for sawn timber production in *Eucalyptus grandis*. **Genet Mol Biol**, 27:567–573, 2004.

SILVA, J. C. D.; CARVALHO, A. M. M. L.; FARIA, B. D. F. H. D. Methods for alleviation and reduction of the effects of growth stresses in *Eucalyptus urophylla*. **Rev Árvore**, 41, 2017.

SOLORZANO, S.; MOYA, R.; MURILLO, O. Early prediction of basic density, shrinking, presence of growth stress, and dynamic elastic modulus based on the morphological tree parameters of *Tectona grandis*. **J Wood Sci**, 58:290–299, 2012.

SUJAN, K. C.; YAMAMOTO, H.; MATSUO, M. *et al*. Is hygrothermal recovery of tension wood temperature-dependent? **Wood Sci Technol**, 50:759–772, 2016.

SUJAN, K. C.; YAMAMOTO, H.; MATSUO, M. U. *et al*. Delayed recovery of growth stress in tension wood induced by drying and subsequent wetting treatment. **Wood Sci Technol**, 52:1049–1060, 2018.

TANAKA, M.; YAMAMOTO, H.; KOJIMA, M. *et al*. The interrelation between microfibril angle (*MFA*) and hygrothermal recovery (HTR) in compression wood and normal wood of *Sugi* and *Agathis*. **Holzforschung**, 68:823–830, 2014.

TANAKA, M.; YAMAMOTO, H.; YOSHIDA, M. *et al*. Retarded recovery of remaining growth stress in *Agathis* wood specimen caused by drying and subsequent re-swelling treatments. **Eur J Wood Prod**, 73:289–298, 2015.

TOBA, K.; YAMAMOTO, H.; YOSHIDA, M. Micromechanical detection of growth stress in wood cell wall by wide-angle X-ray diffraction (WAX). **Holzforschung**, 67:315–323, 2013.

TRUGILHO, P. F.; OLIVEIRA, J. T. D. S. Relationships and estimates of longitudinal growth stress in *Eucalyptus dunnii* at different ages. **Rev Árvore**, 32:723–729, 2008.

UEDA-MATSUO, M.; NIIMI, G.; SUJAN, K. C. *et al*. Hygrothermal recovery of compression wood in relation to elastic growth stress and its physicochemical characteristics. **J Mater Sci**, 51:7956–7965, 2016.

WATANABE, K.; YAMASHITA, K.; NOSHIRO, S. Non-destructive evaluation of surface longitudinal growth strain on *Sugi* (*Cryptomeria japonica*) green logs using near-infrared spectroscopy. **J Wood Sci**, 58:267–272, 2012.

WATANABE, H. Characteristics of Tree Trunk Logs. **Kyushu University, Department of Wood Physics Research Report**, 1967.

WARDROP, A. B. Cellular structure of woody plants, Côté, W. A. Jr. ed., **Syracuse Univ. Press**, New York, pp. 373-390, 1965.

YAMAMOTO, H. Role of the gelatinous layer on the origin of the physical properties of the tension wood. **J Wood Sci**, 50:197–208, 2004.

YAMAMOTO, H.; ABE, K.; ARAKAWA, Y. *et al*. Role of the gelatinous layer (G-layer) on the origin

of the physical properties of the tension wood of *Acer sieboldianum*. **J Wood Sci**, 51:222–233, 2005.

YAMAMOTO, H.; SUJAN, K. C.; MATSUO-UEDA, M. *et al*. Microscopic mechanism of contraction of tension wood G-fiber due to boiling. **Cellulose**, 29:7935–7954, 2022.

YOSHIDA, M.; FUJIWARA, D.; TSUJI, Y. *et al*. Ultraviolet microspectrophotometric investigation of the distribution of lignin in *Prunus jamasakura* differentiated on a three-dimensional clinostat. **J Wood Sci**, 51:448–454, 2005.

YOSHIDA, M.; IKAWA, M.; KANEDA, K.; OKUYAMA, T. Stem tangential strain on the tension wood side of *Fagus crenata* saplings. **J Wood Sci**, 49:475–478, 2003.

YOSHIDA, M.; OHTA, H.; OKUYAMA, T. Tensile growth stress and lignin distribution in the cell walls of black locust (*Robinia pseudoacacia*). **J Wood Sci**, 48:99–105, 2002.

ZANUNCIO, A. J. V.; CARVALHO, A. G.; CARNEIRO, A. D. C. O. *et al*. Characterization of *Eucalyptus* clones subject to wind damage. **Pesq Agropec Bras**, 52:969–976, 2017.

Chapter 3: Radial distribution of tension wood properties in a thick branch of *Zelkova serrata* Makino. A view of G-layer development

3.1 Introduction

In hardwoods, reaction wood is typically formed on the upper side of leaning trunks or branches and is known as tension wood (TW) (Onaka 1949; Clair *et al.* 2003; Ghislain and Clair 2017). TW generates significant tensile growth stress (Okuyama *et al.* 1990, 1994; Clair *et al.* 2003; Washusen *et al.* 2003), contributing to negative gravitropism in woody trunks (Yamamoto *et al.* 2002; Fourcaud and Lac 2003). However, TW causes various processing defects when hardwood logs are used for structural lumber. Sawing green hardwood logs often results in warping, cracking, and splitting of the primary products. These defects are further exacerbated during the subsequent kiln-drying process.

Sawing defects in primary lumber result from the instantaneous release of the elastic component of residual growth stress within the log, whereas the drying defects arise from abnormal shrinkage of TW fibers— specifically, hygrothermal recovery (HTR) at the initial heating stage and drying shrinkage during the subsequent drying stage. These defects significantly reduce the processing yield of the final product (Vilkovská *et al.* 2019; Klement *et al.* 2019). Additionally, researchers suggest that the viscoelastic component of growth stress remains in the cut specimens and is rapidly released by boiling, causing HTR (Abe and Yamamoto 2007; Clair 2012; Sujan *et al.* 2015, 2016; Yamamoto *et al.* 2022; Matsuo-Ueda *et al.* 2023).

As mentioned above, TW exhibits significantly higher growth stress, HTR, and drying shrinkage than normal wood (NW). It is also known that TW has higher cellulose crystallinity and lower cellulose microfibril angle (*MFA*) (Müller *et al.* 2006; Yamamoto *et al.* 2022). Many researchers attribute these properties of TW to the presence of cellulose-rich G-layers formed within the secondary walls of TW fibers (Okuyama *et al.* 1990, 1994; Clair *et al.* 2003; Yamamoto *et al.* 2005).

In recent years, plantations of fast-growing hardwood species have become increasingly common to meet the rising demand for hardwood lumber. These trees are typically harvested at a young age, resulting in relatively small trunk diameters and often irregular trunk shapes. Consequently, the lumber sawn from these logs contains both sapwood and heartwood and frequently exhibits TW. To address defects caused by TW in these materials, it is essential to understand the distribution patterns of TW properties within the trunk from heartwood to sapwood.

However, there is limited information on the continuous variation of wood physical properties within the trunk, from heartwood to sapwood, particularly focusing on TW formation. Therefore, the present study used an inclined thick branch of a keyaki tree (*Zelkova serrata* M) to measure the radial heterogeneity of physical properties from heartwood to sapwood containing TW. Specifically, we examined HTR strain, drying strain, cellulose crystallinity, *MFA* and G-layer proportion across this gradient. Our ultimate goal is to promote the use of lesser-known and small- to medium-diameter hardwood logs for lumber.

3.2 Materials and Methods

3.2.1 Sample preparation and outline of experimental procedure

A basal disk was sampled from a 27-year-old branch with a diameter of 19 cm from a mature keyaki tree (*Zelkova serrata* Makino), grown in Sekigahara Town, Gifu Prefecture, Japan. Keyaki trees are used for traditional constructions such as shrines and temples. Therefore, a relatively large-diameter specimen was used in this study.

Vertical Groups A, B, and C

As shown in Figure 19,
(a) A vertical line was drawn through the pith on the cross-section of the sampled disk. A quartersawn board measuring approximately 50 mm (longitudinal, L) × 15 mm (tangential, T) was cut to include the vertical line.
(b) On the cross-section of the quartersawn board, sampling positions were marked every 5 mm along the radial (R) direction from the pith toward the bark. At each position, rectangular portions measuring 50 mm (L) × 15 mm (T) × 5 mm (R) were prepared.
(c) From each rectangular portion, three specimens measuring 15 mm (L) × 15 mm (T) × 5 mm (R) were cut. The specimens were grouped into Vertical groups A, B, and C, such that the specimens in each group were contiguous along the R-direction.

Horizontal Group D

(d) A horizontal line was drawn through the pith on the cross-section. A quartersawn board measuring 15 mm (L) × 15 mm (T) was then cut to include the horizontal line, excluding the region near the pith that had been used for the Vertical groups.

(e) On the cross-section of the quartersawn board, sampling positions were marked every 5 mm along the R-direction from the pith toward the bark. At each position, rectangular specimens measuring 15 mm (L) × 15 mm (T) × 5 mm (R) were prepared. These specimens were grouped as the Horizontal group D.

Figure 19 - How to prepare specimens

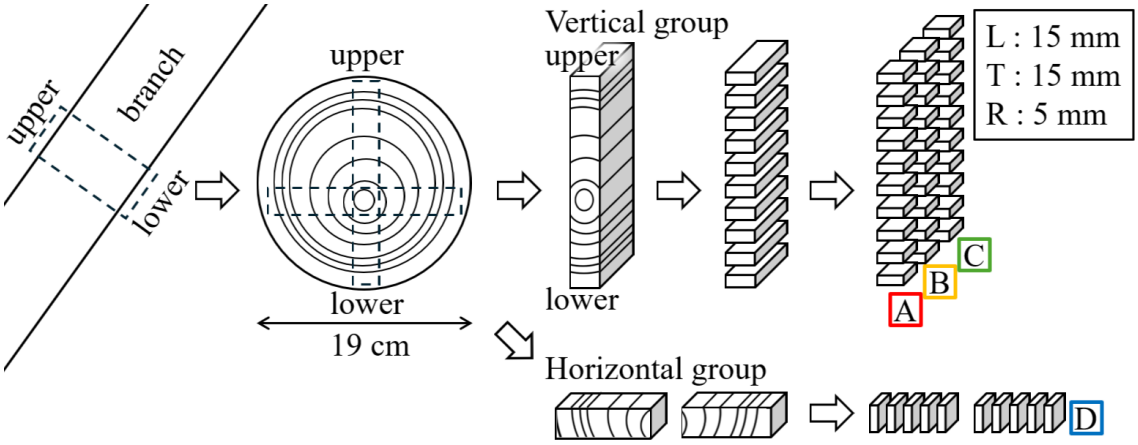

Source: Author's own

In this study, various measurements were conducted on each group, as shown in Figure 20. Vertical group A was used to measure hygrothermal recovery (HTR) strain, cellulose crystallinity index (*C.I.*), microfibril angle (*MFA*), and G-layer proportion. Vertical group B was used for the measurements of drying strain, *C.I.*, *MFA* and G-layer proportion. Vertical group C was used to measure HTR strain, drying strain and *C.I.* Horizontal group D was used to measure HTR strain, *C.I.*, *MFA* and G-layer proportion.

Figure 20 - Measurements procedures for each group

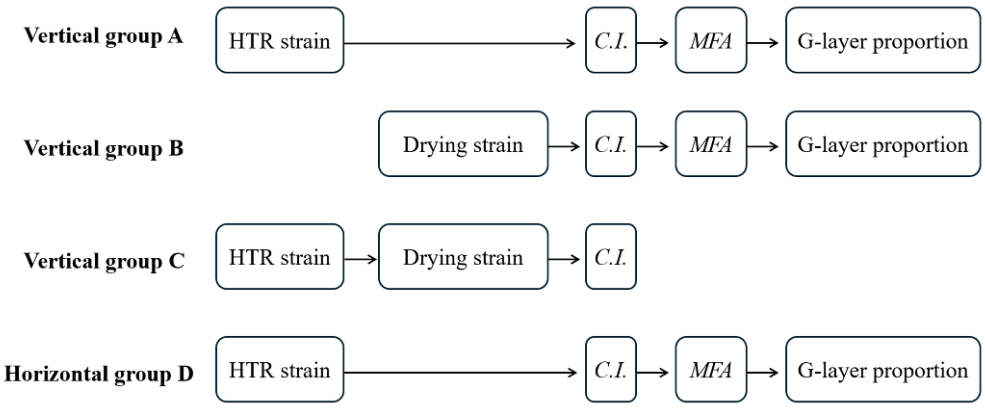

Source: Author's own

3.2.2 HTR strain

For all groups, the L- and T-dimensions in the green condition ($l_L{}^G$ and $l_T{}^G$) were measured at room temperature using a dial-gauge comparator with a reading accuracy of 0.001 mm (see Tanaka *et al.* 2014, *ibid*. 2015). Vertical groups A and C, and Horizontal group D were boiled in hot water (at 120 °C for 40 minutes using an autoclave). After these processes, the L- and T-dimensions ($l_L{}^{HTR}$ and $l_T{}^{HTR}$) were measured at room temperature, and the HTR strains due to boiling (ε_L and ε_T) were calculated as follows:

$$\varepsilon_L = \frac{l_L^{HTR} - l_L^G}{l_L^G} \times 100\ (\%)\ , \qquad \varepsilon_T = \frac{l_T^{HTR} - l_T^G}{l_T^G} \times 100\ (\%). \tag{1}$$

3.2.3 Drying strain

Vertical group B was air-dried for one week from their green condition, followed by oven-drying at 105 °C for 24 hours using a convection oven. The Vertical group C were also dried after boiling. Following these processes, the L- and T-dimensions, $l_L{}^{dry}$ and $l_T{}^{dry}$, were measured, and the drying strains of Vertical group B (α_L and α_T) were calculated as follows:

$$\alpha_L = \frac{l_L^{dry} - l_L^G}{l_L^G} \times 100\ (\%)\ , \qquad \alpha_T = \frac{l_T^{dry} - l_T^G}{l_T^G} \times 100\ (\%) \tag{2}$$

The drying strain of Vertical group C (β_L and β_T) were calculated as follows:

$$\beta_L = \frac{l_L^{dry} - l_L^{HTR}}{l_L^{HTR}} \times 100\ (\%)\ , \qquad \beta_T = \frac{l_T^{dry} - l_T^{HTR}}{l_T^{HTR}} \times 100\ (\%) \tag{3}$$

3.2.4 Wide-angle X-ray scattering (WAXS) for crystallinity index (*C.I.*) and cellulose microfibril angle (*MFA*)

After measuring dimensions, each specimen was divided into two flatsawn pieces measuring 15 mm (L) × 15 mm (T) × 2.5 mm (R), which were air-dried for one week. Following air drying, wide-angle X-ray scattering (WAXS) profiles were obtained using a XRD measurement device (Ultima IV, Rigaku Co. Ltd., Tokyo, Japan) (Figure 21). The crystallinity index (*C.I.*) was then calculated according to Segal's method (Segal *et al.* 1959) as modified by Yamamoto *et al.* (2022) and with reference to French *et al*. (2013), using the following formula in a Jupyter Notebook environment:

$$C.I. = \frac{I_{200} - I_{amor}}{I_{200}} \times 100\ (\%) \tag{4}$$

where I_{200} is the intensity of the 200 diffraction peak, which is fitted by a Lorentzian function, and

I_{amor} is the intensity of the amorphous scattering around 2θ = 18°, which is fitted by a quadratic function, after subtracting the background intensity from the original profile.

Figure 21 - Typical WAXS profiles of (a) TW and (b) OW of keyaki tree used in the present study. The background has been removed from the original profiles.

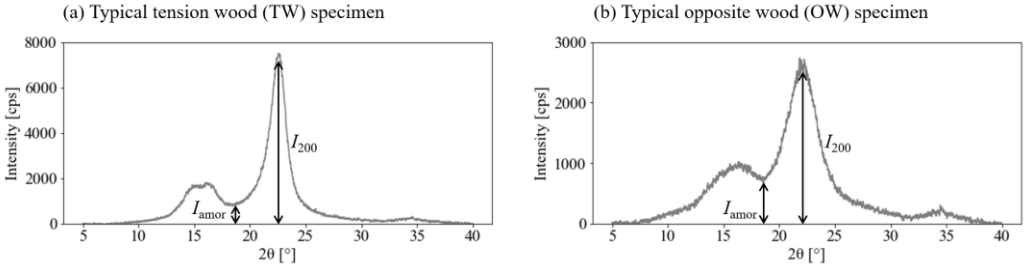

Source: Author's own

After obtaining *C.I.*, β profiles were derived (Yamamoto *et al.* 2022). Angle *T*, which provides an estimate of the average *MFA*, was determined from the β profiles (Cave 1966). As shown in Figure 22, tangent line was drawn at the inflection point Q. The intersection point R between the tangent line and the base line (y=0), as well as the intersection point O between the symmetrical line and the base line (y=0) were identified. The distance OR is defined as Angle *T* (°). The peak profiles were fitted with a pseudo-Voigt function. The *MFA* were then calculated as follows (Cave 1966) in a Jupyter Notebook environment:

$$MFA(°) = 0.6 \times \text{Angle } T. \quad (5)$$

Yamamoto *et al.* (1993) and Tanaka *et al.* (2014) demonstrated that Cave's method can be applied when angle *T* ranges approximately from 15° to 40°. In the present study, although a few specimens exhibited small angle *T* values as low as 13°, all calculations were performed using Cave's method Eq. (5) for simplicity.

Figure 22 - Typical β profiles of (a) TW and (b) OW of keyaki tree used in the present study. The background has been removed from the original profile.

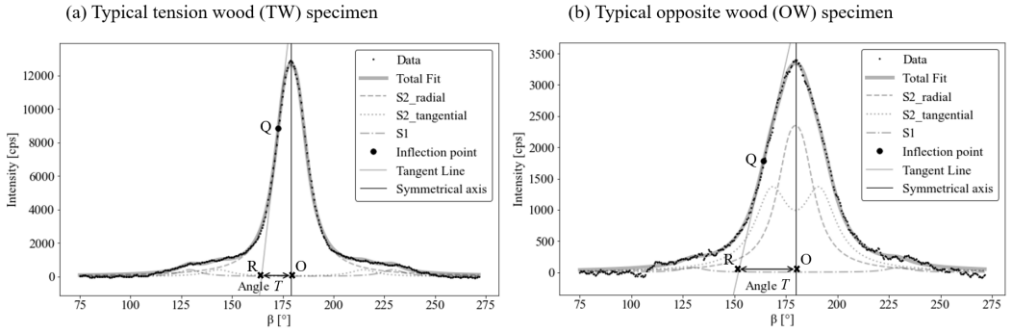

Source: Author's own

3.2.5 Microscopy observation and G-layer proportion

After *MFA* measurements, the specimen was swollen in water, and cross-sections with thicknesses of 14-18 μm were prepared from Vertical groups A and B, and Horizontal group D, using a sliding microtome (Yamato, blade type S35). The sections were first stained with a 1% aqueous safranin solution, then dehydrated through a graded ethanol series. Upon reaching 95% ethanol, they were stained with a 1% ethanolic fastgreen solution, followed by final dehydration in 100% ethanol. The stained sections were then cleared with Lemosol and mounted using Entellan® New (Merck, Darmstadt, Germany; Cat. No. 1.07961.0100).

Observations were conducted using a light microscope (BX53, Olympus, Tokyo, Japan). The presence of the G-layer was initially confirmed through high-magnification observations (10×–40×) (Figure 23). Subsequently, microscopic images covering the entire section were captured at 4× objective magnification and stitched together using Process Manager (cellSens [Ver. 4.2.1], Olympus), enabling the reconstruction of wide-field images from multiple adjacent fields of view. As shown in Figure 24, G-layer proportion in microscopic images of each specimen was measured by adjusting the HSV (Hue, Saturation, Value) range to (50, 50, 50)–(120, 255, 255) to extract the fastgreen–stained areas (i.e., G-layer regions) from the entire cross-section of the specimen.

Figure 23 - Well-developed G-layer, (b) partially-developed G-layer, and (c) poorly-developed G-layer of keyaki tree used in the present study. The scale bars in the lower right corner of the images represent 40 μm.

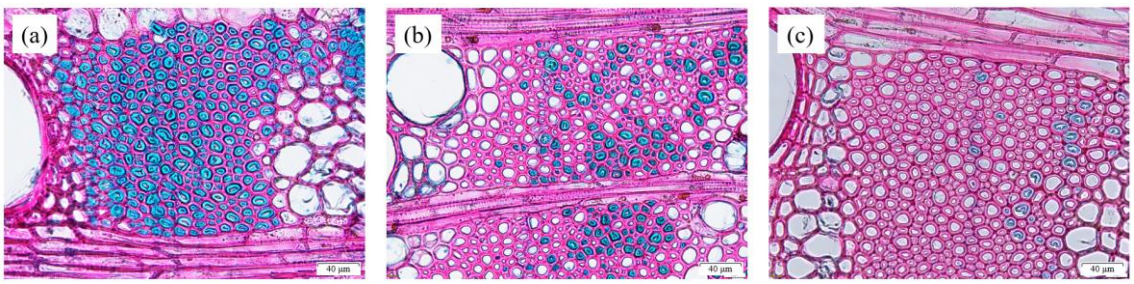

Source: Author’s own

Figure 24 - (a) Captured image showing well-developed G-layer, and (b) image with the fast-green stained area extracted (highlighted in green). The G-layer proportion in this specimen was 57%. (c) Captured image showing partially developed G-layer, and (d) image with the fast-green stained area extracted (highlighted in green). The G-layer proportion in this specimen was 13%.

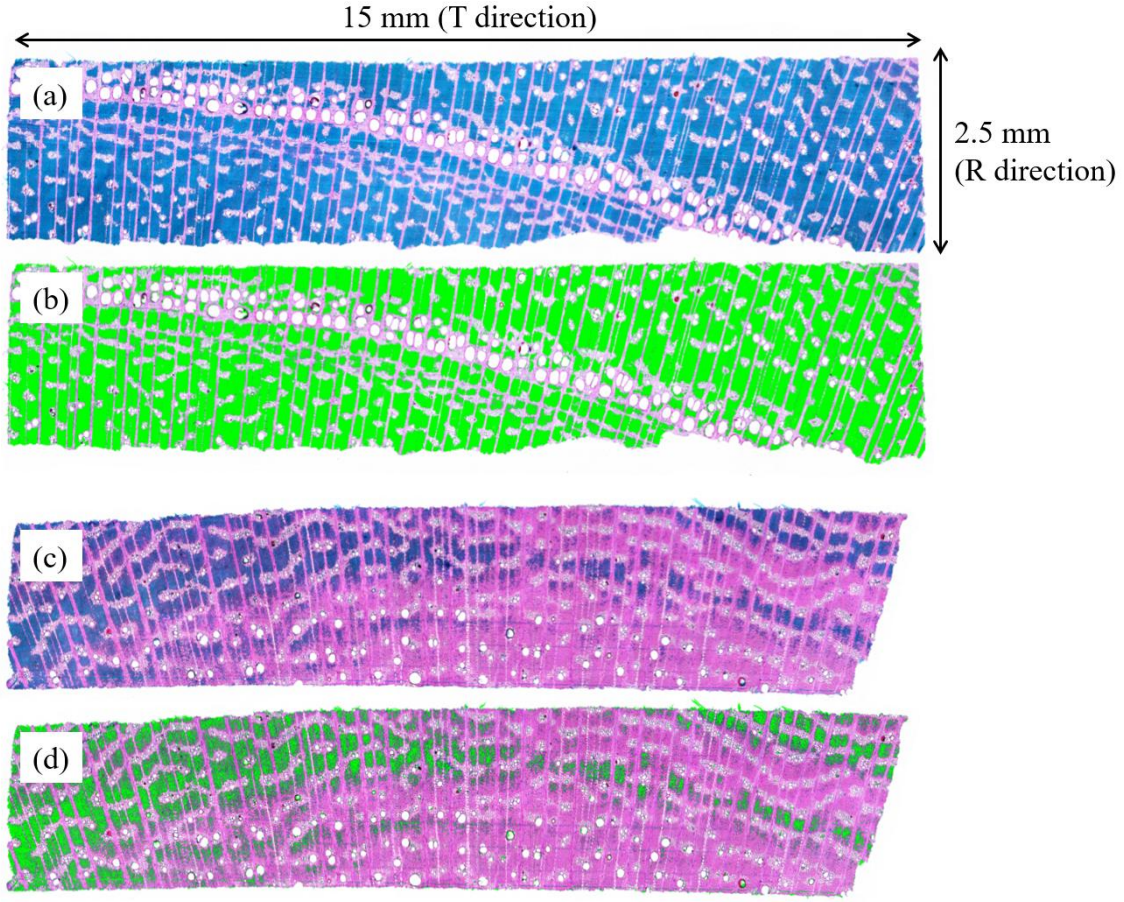

Source: Author's own

G-layer proportion (g) was calculated as follows:

$$g = \frac{\text{Pixel count of the region extracted as G-layer}}{\text{Pixel count of the entire section}} \times 100\ (\%). \qquad (6)$$

3.3 Results and Discussion

3.3.1 Vertical groups A, B, and C

TW formation, C.I., and MFA

G-layer proportion in Vertical groups A and B was higher on the upper side of the branch, indicating that TW-fiber was formed on the upper side of the branch. Similarly, *C.I.* in Vertical groups A, B and C was also higher, and *MFA* in vertical groups A and B was lower on the upper side (Figure 25). Those were nearly uniform regardless of the distance from the pith. These results suggest that both *C.I.* and *MFA* directly reflect the degree of G-layer development.

Although the G layer proportion was not measured in Vertical group C, the specimens in Vertical group C were taken from fibers longitudinally aligned with those in Vertical groups A and B. Therefore, it is reasonable to assume that TW also formed on the upper side in group C. In fact, the radial distribution *C.I.* of Vertical group C exhibited a trend similar to that of Vertical groups A and B as described below.

Figure 25 - Radial distributions of *C.I.*, and *MFA* in comparison with G-layer proportion

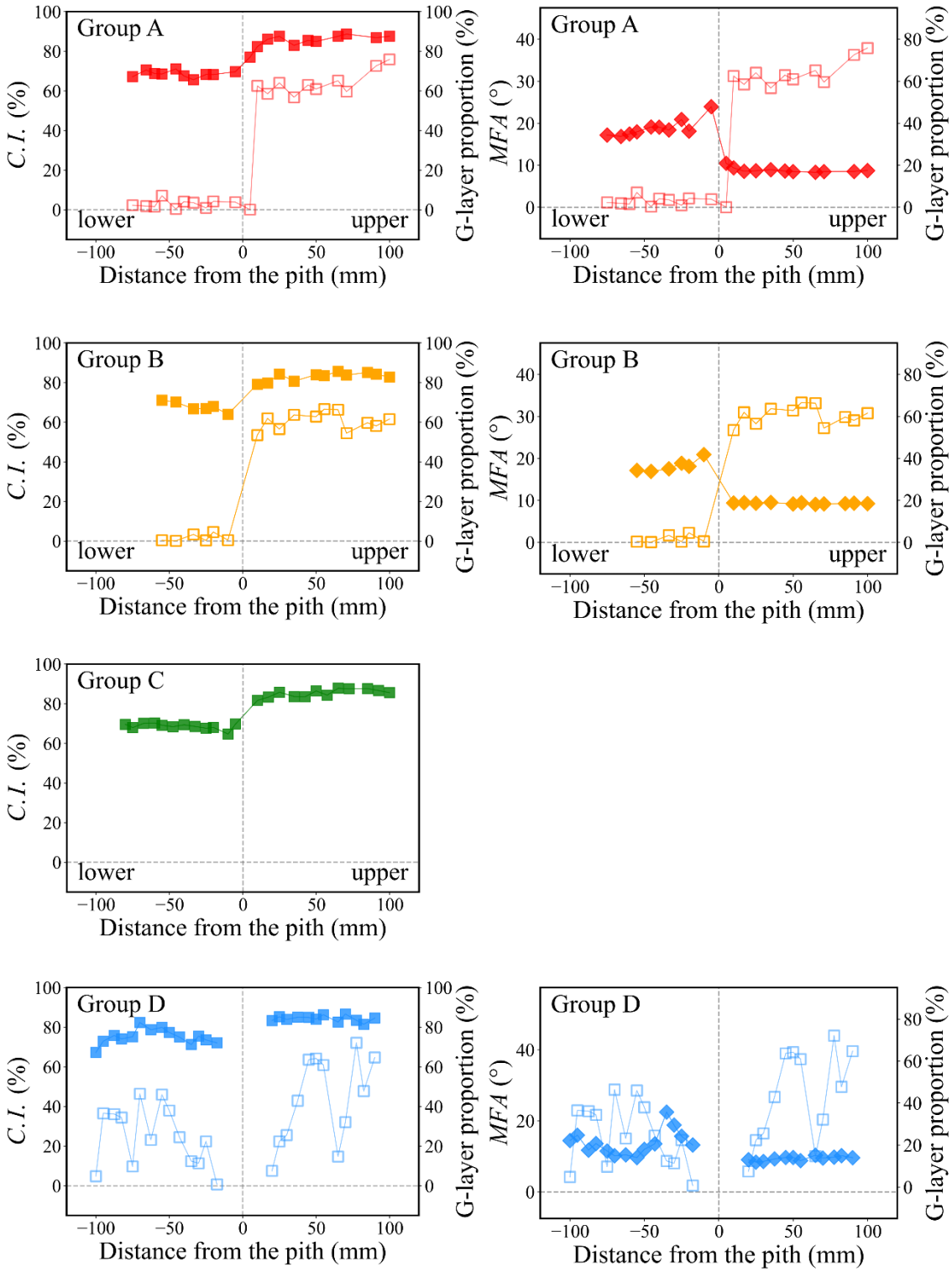

Source: Author's own

Drying strain

The drying strain in the L-direction of Vertical groups B and C exhibited a greater negative (contractive) value on the upper side of the branch, while it was nearly zero or slightly positive (expansive) on the lower side (Figure 26). The drying strain in the T-direction also showed a more pronounced negative value on the upper side of the branch, with a relatively smaller negative value on the lower side (Figure 26). These differences between the upper and lower sides are consistent with previous studies where specimens were taken around the circumference of disks (Clair *et al.* 2003; Abe and Yamamoto 2007). The drying strain was almost uniform on both the upper and lower sides of the branch, regardless of the distance from the pith. Therefore, the drying strain is primarily determined by the G-layer proportion, with minimal dependence on the distance from the pith.

No clear difference was observed in the drying strain in the L-direction between groups B and C on either the upper or lower sides of the branch. However, the contractive drying strain in the T-direction was slightly greater in group C than in group B on both sides. This heightened T-strain in group C likely results from the boiling treatment preferentially softening or partially leaching amorphous hemicelluloses/lignin (matrix components), thereby removing the restraint on the highly hygroscopic cellulose structure, allowing for greater collapse in the T-direction upon drying. From these results, it can be considered that the HTR can be release growth stress in the L-direction but also causes grater collapse in the T-direction subsequent drying.

Figure 26 - Radial distributions of drying strains (L, T) in comparison with G-layer proportion

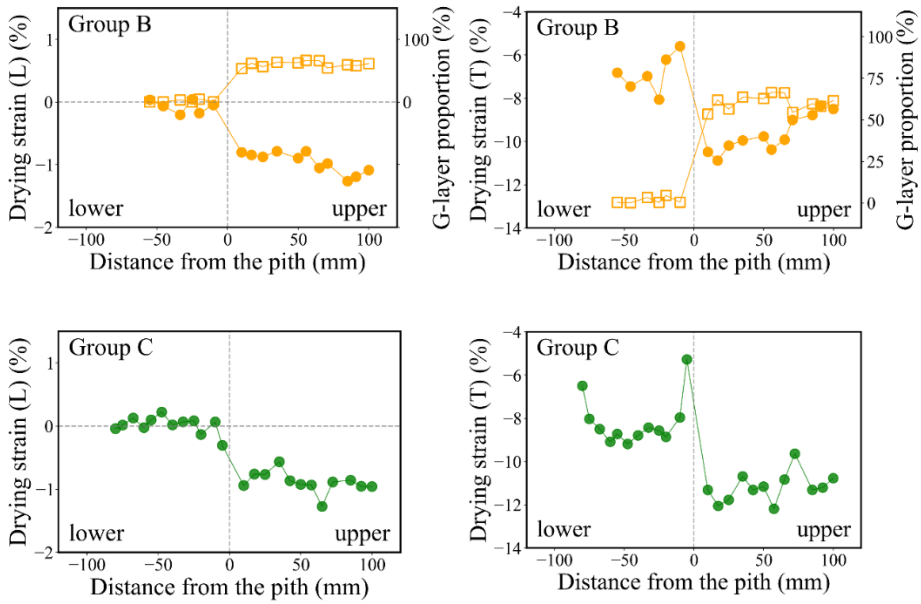

Source: Author's own

HTR strain

HTR strain in the L-direction of Vertical groups A and C exhibited the maximum negative (contractive) strain near the bark on the upper side of the branch. The absolute value of the HTR strain decreased monotonically and became positive (expansive) as it approached the pith, ultimately reaching the maximum positive strain near the pith. On the lower side of the branch, the HTR strain in the L-direction was nearly zero or slightly positive near the bark and showed the maximum positive strain near the pith (Figure 27).

The HTR strain in the T-direction of Vertical groups A and C exhibited maximum positive strain near the bark on the upper side of the branch, which gradually decreased toward the pith and showed a slight negative strain near the pith. On the lower side of the branch, the HTR strain was positive near the bark but somewhat smaller than that observed on the upper side (Figure 27).

The HTR strain in the L-direction exhibited a mountain-shaped distribution, whereas in the T-direction, it displayed a valley-shaped distribution (Figure 27). These variations, depending on the distance from the pith, are consistent with previous studies on sugi trees (*Cryptomeria japonica* D.) (Sasaki and Okuyama 1983; Kitahara *et al.* 1986). Therefore, it can be suggested that HTR depends not only on the G-layer proportion but also on the distance from the pith, regardless of whether the wood is softwood or hardwood. This point will be discussed again later.

Figure 27 - Radial distributions of HTR strains (L, T) in comparison with G-layer proportion

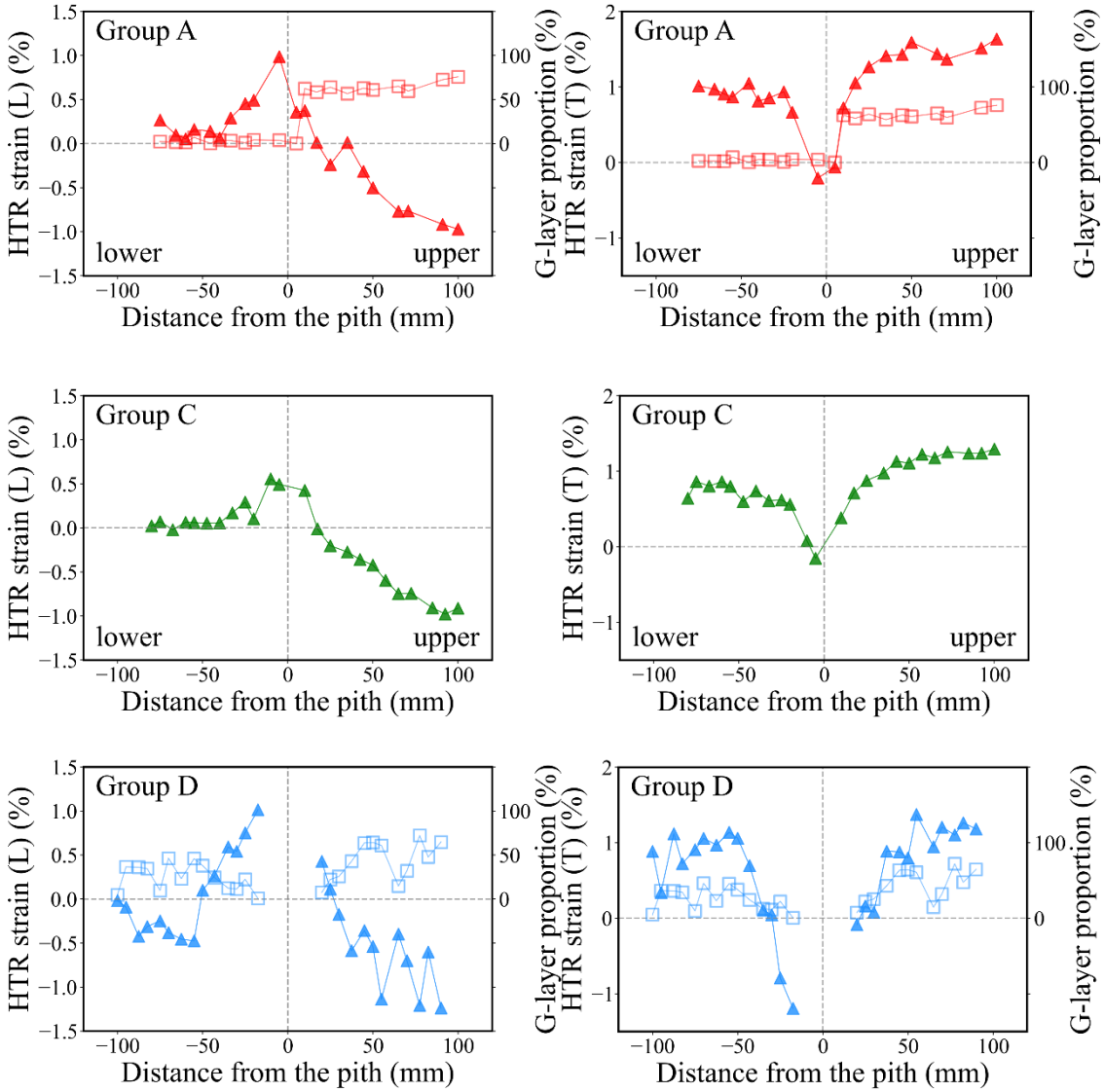

Source: Author's own

3.3.2 Horizontal group D

TW formation, C.I., and MFA

Unlike the case in Vertical groups, Horizontal group included specimens that exhibited a medium G-layer proportion. Horizontal group D showed a slightly higher G-layer proportion on the right side of the x-axis compared to the left side. *C.I.* and *MFA* also displayed similar trends to the G-layer proportion (Figure 25).

HTR strain

The HTR strain in the L-direction of Horizontal group D exhibited the maximum negative strain near the bark. Near the bark, HTR strain showed contraction (negative), while near the pith it showed extension (positive). In between, the strain transitioned from negative to positive (Figure 27).

The HTR strain in the T-direction of Horizontal group D exhibited larger positive values near the bark, which decreased toward the pith, reaching the maximum negative value at the innermost position (Figure 27).

Like Vertical groups, the HTR strain in the L- and T-directions exhibited mountain- and valley-shaped distributions, respectively. This indicates that the HTR strain depends on the distance from the pith, regardless of whether the groups are Vertical or Horizontal (Figure 27).

3.3.3 Correlation between G-layer proportion and various measurements

Figure 28 (a) shows the correlation between the G-layer proportion and *C.I.* in Vertical groups A and B, with an *R*-squared value of 0.73. Figure 28 (b) illustrates the correlation between the G-layer proportion and *MFA* in Vertical groups A and B, with an *R*-squared value of 0.63. Figure 28 (c) depicts the correlation between the G-layer proportion and the HTR strain in the L-direction in Vertical group A and Horizontal group D, with an *R*-squared value of 0.53. Figure 28 (d) shows the correlation in the T-direction for Vertical group A and Horizontal group D, with an *R*-squared value of 0.32.

The correlation between *C.I.*, *MFA*, and the HTR strain with the G-layer proportion was highest for *C.I.*, followed by *MFA*, and lowest for the HTR strain. These results suggest that *C.I.* and *MFA* are primarily influenced by TW associated with the G-layer proportion and minimally affected by the distance from the pith. In contrast, the HTR strain is influenced both by TW and by other factors related to the distance from the pith, such as the distribution of residual growth stress. Indeed, previous studies on conifers (Sasaki and Okuyama 1983; Kitahara *et al.* 1986) have demonstrated that HTR reflects the history of growth stress generation in the xylem and its accumulation during radial growth. The lower correlation of HTR strain with the G-layer proportion is not a limitation but the primary evidence of HTR's superiority as a metric. It confirms that the HTR strain is a measure of the complex, accumulated stress history of the wood—an inherently dynamic quantity influenced by distance from pith—rather than merely a static anatomical feature like *C.I.* or G-layer area. This establishes HTR as a dynamic-history metric and a more reliable tool for predicting eventual warping defects than simple anatomical indices alone.

For reference, Figure 28 (e) shows the correlation between the G-layer proportion and the drying strain in the L-direction for vertical group B, and Figure 28 (f) shows the correlation in the T-direction for vertical group B. Because there is no data set for specimens with a medium G-layer proportion, it is not possible to easily discuss the correlation, but we have calculated the apparent *R*-squared values for Figure 28 (e) and (f). The values obtained are quite high, at 0.89 and 0.73, respectively. This is mainly because the data set is clearly divided into two different groups: TW, which has a high G-layer proportion with a large contractive drying strain, and NW, which has a zero or low G-layer proportion but a small drying strain.

Figure 28 - Correlation between *C.I.*, *MFA*, HTR strains (L, T), drying strains (L, T) and G layer proportion

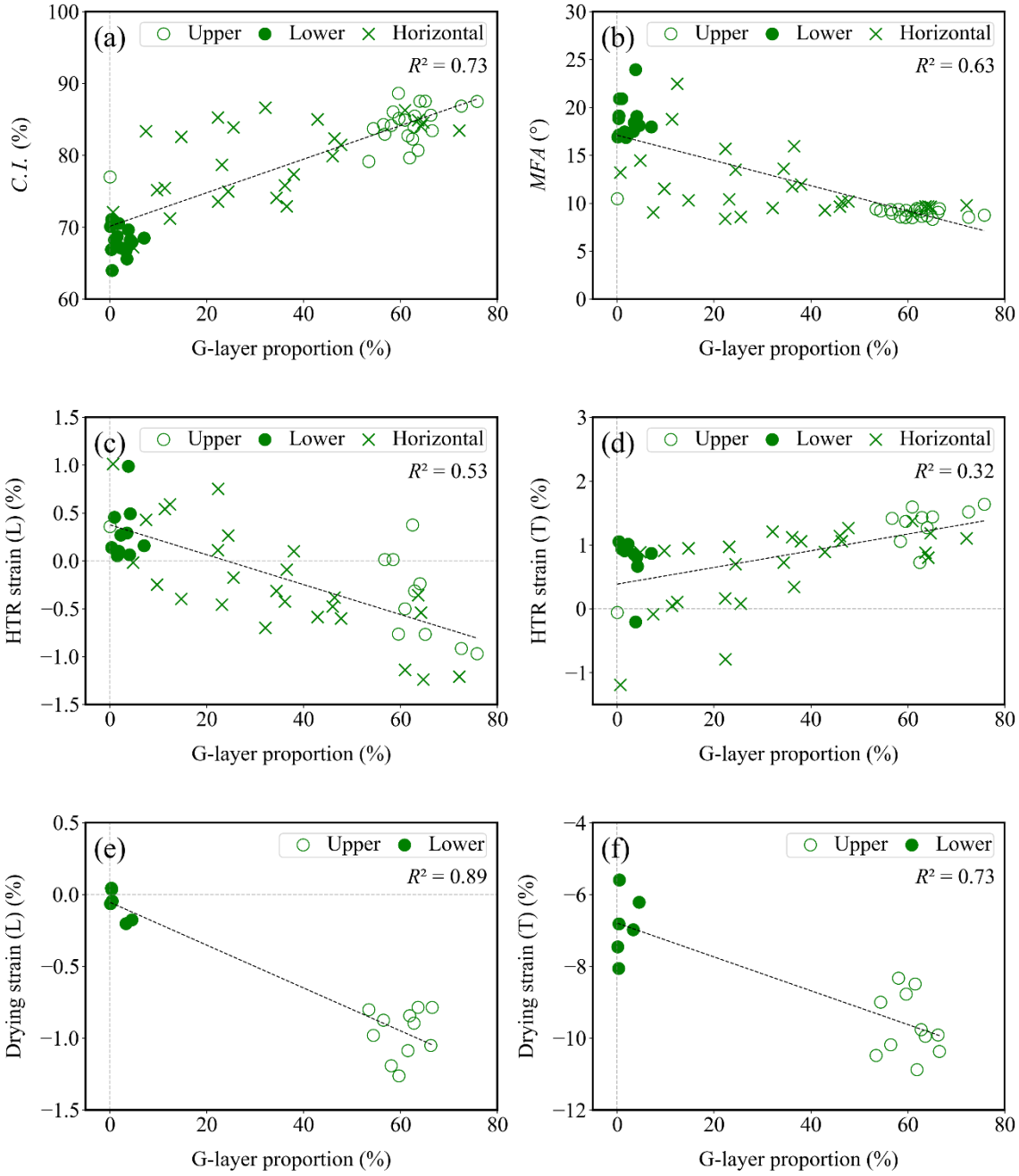

Source: Author's own

3.4 Conclusion

In this study, using a thick branch of a keyaki tree, HTR strain, drying strain, *C.I.*, *MFA*, and G-layer proportion were measured vertically and horizontally along the radial direction on the cross-section.

On the upper half of the inclined branch, higher G-layer proportion was observed, confirming the formation of TW. *C.I.*, *MFA*, and the drying strain exhibited behaviors characteristic of TW on the upper side. The comparison of correlations between *C.I.*, *MFA*, and the HTR strain with the G-layer proportion was highest for *C.I.*, followed by *MFA*, and lowest for the HTR strain.

Considering the radial distribution patterns of these traits, it is suggested that *C.I.* and *MFA* are primarily affected by TW, which is related to the G-layer proportion, and that the distance from the pith has a small effect. Although there is little data, the same can be said about the drying strain as for *MFA* and *C.I.* On the other hand, the HTR strain is influenced not only by TW but also by other factors such as growth stress, suggesting that HTR reflects the history of growth stress generation in the xylem and its accumulation during radial growth.

To improve hardwood lumber processing, it is essential to understand the mechanisms of growth stress and other TW properties in relation to the G-layer.

Reference

ABE, K.; YAMAMOTO, H. The influences of boiling and drying treatments on the behaviors of tension wood with gelatinous layers in *Zelkova serrata*. **J Wood Sci**, 53:5–10, 2007.

CAVE, I. D. Theory of X-Ray Measurement of Microfibril Angle in Wood. **Forest Products Journal**, 16:37–42, 1966.

CLAIR, B. Evidence that release of internal stress contributes to drying strains of wood. **Holzforschung**, 66:349–353, 2012.

CLAIR, B.; RUELLE, J.; THIBAUT, B. Relationship between growth stress, mechanical-physical properties and proportion of fibre with gelatinous layer in chestnut (*Castanea sativa* Mill.). **Holzforschung**, 57:189–195, 2003.

FOURCAUD, T.; BLAISE, F.; LAC, P. *et al*. Numerical modelling of shape regulation and growth stresses in trees. **Trees**, 17:31–39, 2003.

FOURCAUD, T.; LAC, P. Numerical modelling of shape regulation and growth stresses in trees. **Trees**, 17:23–30, 2003.

FRENCH, A. D.; CINTRON, M. S. Cellulose polymorphy, crystallite size, and the Segal Crystallinity Index. **Cellulose**, v. 20, p. 583-588, 2013.

GHISLAIN, B.; CLAIR, B. Diversity in the organisation and lignification of tension wood fibre walls – A review. **IAWA Journal**, 38:245–265, 2017.

KITAHARA, R.; TSUTSUMI, J.; MATSUO, T. Wood deformations due to growth stress release. **Bulletin of the Utsunomiya University Forests**, 22:49–60, 1986.

KLEMENT, I.; VILKOVSKÁ, T.; UHRÍN, M. *et al*. Impact of high temperature drying process on beech wood containing tension wood. **Open Engineering**, 9:428–433, 2019.

MATSUO-UEDA, M.; YOSHIDA, M.; YAMAMOTO, H. Analysis of hygrothermal recovery of tension wood induced by boiling at 50–80 °C. **Holzforschung**, 77:270–282, 2023.

METZGER, K. Über das Konstruktionsprinzip des sekundären Holzkörpers. **Naturwissenschaftliche Zeitschrift für Forst- und Landwirtschaft**, 6:249–278, 1908.

MÜLLER, M.; BURGHAMMER, M.; SUGIYAMA, J. Direct investigation of the structural properties of tension wood cellulose microfibrils using microbeam X-ray fibre diffraction. **Holzforschung**, 60:474–479, 2006.

OKUYAMA, T.; YAMAMOTO, H.; MASAKI, I.; MASATO, Y. Generation process of growth stresses in cell walls II. Growth stresses in tension wood. **Mokuzai Gakkaishi**, 36:797–803, 1990.

OKUYAMA, T.; YAMAMOTO, H.; YOSHIDA, M. *et al*. Growth stresses in tension wood: role of microfibrils and lignification. **Ann For Sci**, 51:291–300, 1994.

ONAKA, F. Studies on compression- and tension-wood. **Wood Research**, 1:1–88, 1949.
SASAKI, Y.; OKUYAMA, T. Residual stress and dimensional changes on heating green wood. **Mokuzai Gakkaishi**, 29:302–307, 1983.

SEGAL, L.; CREELY, J. J.; MARTIN, A. E.; CONRAD, C. M. An empirical method for estimating the degree of crystallinity of native cellulose using the X-ray diffractometer. **Textile Research Journal**, 29:786–794, 1959.

SUJAN, K.; YAMAMOTO, H.; MATSUO, M. *et al*. Continuum contraction of tension wood fiber induced by repetitive hygrothermal treatment. **Wood Sci Technol**, 49:1157–1169, 2015.

SUJAN, K. C.; YAMAMOTO, H.; MATSUO, M. *et al*. Is hygrothermal recovery of tension wood temperature-dependent? **Wood Sci Technol**, 50:759–772, 2016.

TANAKA, M.; YAMAMOTO, H.; KOJIMA, M. *et al*. The interrelation between microfibril angle (*MFA*) and hygrothermal recovery (HTR) in compression wood and normal wood of *Sugi* and *Agathis*. **Holzforschung**, 68:823–830, 2014.

VILKOVSKÁ, T.; KLEMENT, I.; ČUNDERLÍK, I. Longitudinal contraction of reaction and opposite wood during drying process. **Wood Research**, 64:903–912, 2019.

WASHUSEN, R.; ILIC, J.; WAUGH, G. The relationship between longitudinal growth strain and the occurrence of gelatinous fibers in 10- and 11-year-old *Eucalyptus globulus* Labill. **Holz als Roh- und**

Werkstoff, 61:299–303, 2003.

YAMAMOTO, H.; ABE, K.; ARAKAWA, Y. *et al*. Role of the gelatinous layer (G-layer) on the origin of the physical properties of the tension wood of *Acer sieboldianum*. **J Wood Sci**, 51:222–233, 2005.

YAMAMOTO, H.; OKUYAMA, T.; YOSHIDA, M. Method of determining the mean microfibril angle of wood over a wide range by the improved Cave's method. **Mokuzai Gakkaishi**, 39:375–381, 1993.

YAMAMOTO, H.; SUJAN, K. C.; MATSUO-UEDA, M. *et al*. Microscopic mechanism of contraction of tension wood G-fiber due to boiling. **Cellulose**, 29:7935–7954, 2022.

YAMAMOTO, H.; YOSHIDA, M.; OKUYAMA, T. Growth stress controls negative gravitropism in woody plant stems. **Planta**, 216:280–292, 2002.

Chapter 4: Mechanism of Growth Stress Generation inferred from Hygrothermal Recovery Behavior of Hardwoods including Tension wood

4.1 Introduction

Wood is an important resource for sustainability and is used for furniture and building materials. During lumber processing including sawing, boiling and drying, wood may warp and crack. These deformation causes yield loss of up to 30% (FAO, 1966) and caused by releasing growth stress (Kitahara *et al.* 1986; Gril *et al.* 2017).

Growth stress is influenced by tree growth and environmental conditions. To grow taller, a tree generates surface growth stress, a tensile and compressive force along the longitudinal (L) and tangential (T) direction, respectively, formed just inside the cambium. As the tree matures, the stem thickens, and surface growth stresses accumulate, resulting in residual growth stress. Residual growth stress has tensile stress near the bark and compressive stress near the pith. On a slope, hardwood forms a G-layer at the innermost part of the wood fiber on the upper side of the stems to induce negative gravitropism (Yamamoto *et al.* 2002). The G-layer generates stronger surface growth stress(Okuyama *et al.* 1994; Yoshida *et al.* 2002).

In this way, the standing tree is mechanically balanced, but this balance is disturbed by falling, sawing, and boiling, leading to the release of growth stress, which occurs in two stages. When a tree is felled, the elastic components of residual growth stress are instantaneously released. Subsequently, the viscoelastic components are released over a long period. However, these components can also be released in a shorter time by boiling. The release of growth stress through boiling is referred to as hygrothermal recovery (HTR) (Gril and Thibaut 1994; Abe and Yamamoto 2006; Bardet *et al.* 2012; Capron *et al.* 2018; Chen *et al.* 2020, 2021; Yamamoto *et al.* 2022; Matsuo-Ueda *et al.* 2023).

HTR has been studied from macroscopic behaviors such as dimensional changes to microscopic behaviors at the level of cellulose crystals (Abe *et al.*, 2005, 2006 and 2007; Toba *et al.*, 2013). However, its mechanism has not yet been clarified. The objective in this study is to understand the mechanism of HTR in cellulose crystal level.

4.2 Materials and methods

4.2.1 Sample preparation and outline of experimental procedure

A basal disk was sampled from a 38-year-old, keyaki tree (Zelkova serrata Makino) with a leaning trunk diameter of 16 cm at the Gifu Prefectural Research Institute for Forests, Gifu Prefecture, Japan. Keyaki trees are used for traditional constructions such as shrines and temples. Therefore, a relatively large-diameter specimen was used in this study.

As shown in Figure 29, disks were cut from the trunk, and numerous quarter-sawn strips with dimensions of approximately 80 mm in the longitudinal (L), 15 mm in the tangential (T), and 5 mm in the radial (R) directions were prepared from various positions in the sapwood. These strips were randomly divided into Group A and Group B.

For Group A, four to five specimens measuring 15 (L) × 15 (T) × 5 (R) mm were prepared from each strip. After measuring the green dimensions in the L and T directions, the specimen closest to the upper end was heated to 100℃ for a cumulative 5000 min and subsequently to 120℃ for 3000 min. The time-dependent evolution in hygrothermal recovery strain (HTR strain), expressed as elongation relative to the green dimensions, was recorded. For the remaining specimens, the oven-dry mass was first determined, and then, in order from the upper end, the specimens were boiled for a cumulative 4000 min at 120 °C, 100 °C, 80 °C, or 60 °C. The time-dependent evolution of drying mass, expressed as a percentage of the green oven-dry mass, was measured.

For Group B, the prepared strips were randomly divided into four subgroups (a–d). From each strip, four to five specimens measuring 15 (L) × 15 (T) × 5 (R) mm were cut. Among the specimens contiguous in the L direction, the one closest to the upper end was air-dried at room temperature to obtain profiles of wide-angle X-ray (WAXS). The green L and T dimensions of the remaining specimens were measured. All specimens were then subjected to boiling treatment for a cumulative 4000 min, during which the time-dependent evolutions in both crystallinity index (*C.I.*), the crystallite size (*L*), *d-spacing* (*d*), and HTR strain were determined. The treatment temperatures for subgroups a, b, c, and d were 120 °C, 100 °C, 80 °C, and 60 °C, respectively. *C.I.* measurements were performed under air-dry conditions.

The specimens for measuring HTR strain and *C.I.* were separated because HTR has been reported to occur even under repeated wetting and drying cycles(Tanaka *et al.* 2015; Sujan *et al.* 2018).

Figure 29 - How to prepare specimens

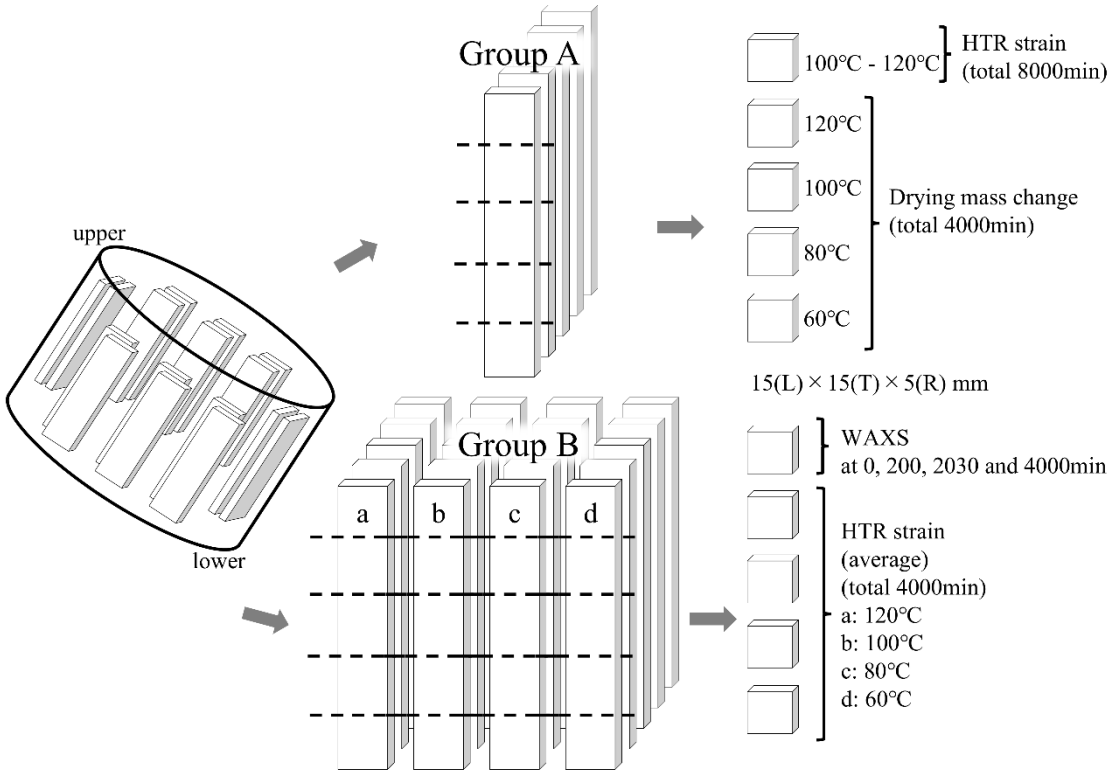

Source: Author's own

4.2.2 HTR strain

First, the L- and T-dimensions in the green condition ($l_L{}^G$ and $l_T{}^G$) were measured at room temperature using a dial-gauge comparator with a reading accuracy of 0.001 mm (see Tanaka *et al.* 2014, *ibid.* 2015). After boiling and cooling in running water, the L- and T-dimensions ($l_L{}^{HTR}$ and $l_T{}^{HTR}$) were measured at room temperature. These boiling, cooling and measuring processes were repeated until the cumulative time reached 8000 and 4000 min in Group A and Group B, respectively. HTR strains due to boiling (ε_L and ε_T) were calculated as follows:

$$\varepsilon_L = \frac{l_L^{HTR} - l_L^G}{l_L^G} \times 100\ (\%)\ , \qquad \varepsilon_T = \frac{l_T^{HTR} - l_T^G}{l_T^G} \times 100\ (\%). \tag{7}$$

4.2.3 Drying mass change

Green specimens were air dried for 3 days, oven dried at 60°C for 1 days and oven dried at 105°C for 7 hours. Then, specimens were cooled in for 15 min in a sealed container and drying mass (m_0) were

measured at room temperature using a convection oven. After boiling, specimens were dried and cooled as mentioned earlier. Then, drying mass (m_t) were measured at room temperature. These drying, boiling, cooling and measuring processes were repeated until the cumulative time reached 4000 in Group A. Drying mass change due to boiling (Δm) were calculated as follows:

$$\Delta m = \frac{m_t - m_0}{m_0} \times 100\ (\%) \tag{8}$$

4.2.4 Wide-angle X-ray scattering (WAXS)

After air-drying the green specimens, wide-angle X-ray scattering (WAXS) profiles were obtained using an XRD measurement device (Ultima IV, Rigaku Co. Ltd., Tokyo, Japan) (Figure 30). WAXS profiles were measured on both sides of each specimen at 200, 2030, and 4000 min following boiling and air-drying. The profiles were fitted with a pseudo-Voigt function. Each parameter — Crystallinity index (*C.I.*), the crystallite size (*L*) and *D-spacing* — was calculated in a Jupyter Notebook environment.

Crystallinity index (*C.I.*) was calculated according to Segal's method (Segal *et al.* 1959) as modified by Yamamoto *et al.* (2022), using the following formula:

$$C.I. = \frac{I_{200} - I_{amor}}{I_{200}} \times 100\ (\%) \tag{9}$$

where I_{200} is the intensity of the 200 diffraction peak, and I_{amor} is the intensity of the amorphous scattering around 2θ = 18° after subtracting the background intensity from the original profile.

The crystallite size (*L*) was estimated using the Scherrer equation:

$$L = \frac{K\lambda}{FWHM \cos\theta}\ (nm) \tag{10}$$

where *L* is the crystallite size, *K* is the shape factor (typically 0.9), λ is the X-ray wavelength, *FWHM* is the full width at half maximum of the diffraction peak in radians, and θ is half of the 2θ value of I_{200}.

D-spacing was calculated according to Bragg's law, using the following formula:

$$d - spacing = \frac{n\lambda}{2 \sin\theta}\ (nm) \tag{11}$$

where *n* is the diffraction order, λ is the X-ray wavelength, and θ is half of the 2θ value of I_{200}.

Figure 30 - Typical WAXS profiles of TW (a) and OW (b) of Zelkova serrata M. used in the present study. The background has been removed from the original profiles.

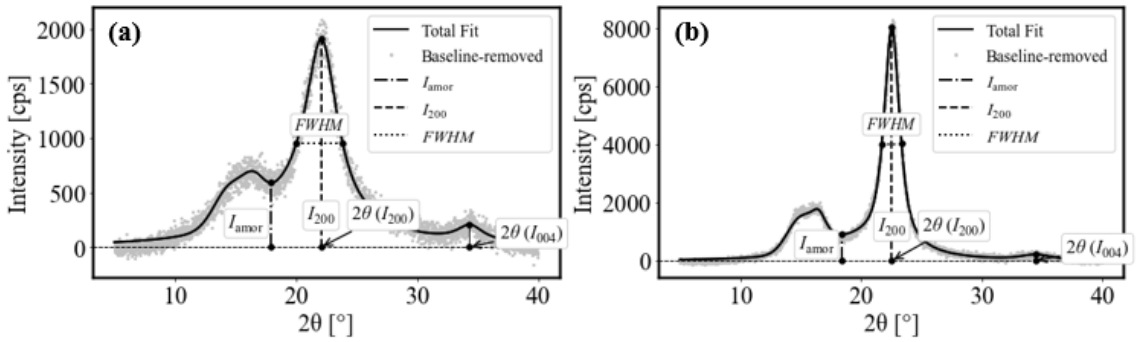

Source: Author's own

4.3 Results and discussion

4.3.1 HTR strain and drying mass change of Group A

HTR strain

Figure 31 (a) shows the time-dependent evolution of HTR strain (L) from 0 to 8000 min, and Figure 31 (b) shows the time-dependent evolution of HTR strain (L) from 0 to 200 min in Group A. In Figure 31 (b), specimens that shrank at the beginning of the boiling treatment (likely TW) and specimens that did not shrink (likely opposite wood, OW) were observed. The variation in shrinkage among the TW specimens is considered to reflect difference in the degree of TW development. In Figure 31 (a), when the treatment temperature was increased to 120 °C at 5000 min, OW specimens also began to shrink linearly. Figure 31 (c) shows the time-dependent evolution of HTR strain (T) from 0 to 8000 min, and Figure 31 (d) shows the time-dependent evolution of HTR strain (T) from 0 to 200 min in Group A. It was observed that TW specimens with larger shrinkage in HTR strain (L) at 8000min in Figure 31 (a) tended to exhibit greater elongation at the beginning of boiling. When the treatment temperature was raised to 120 °C at 5000 min, all specimens began to shrink thereafter. OW showed a transition to shrinkage beyond 6500 min, with the dimensions becoming smaller than in the green state.

Figure 31 - Time-dependent evolution of HTR strain in Group A

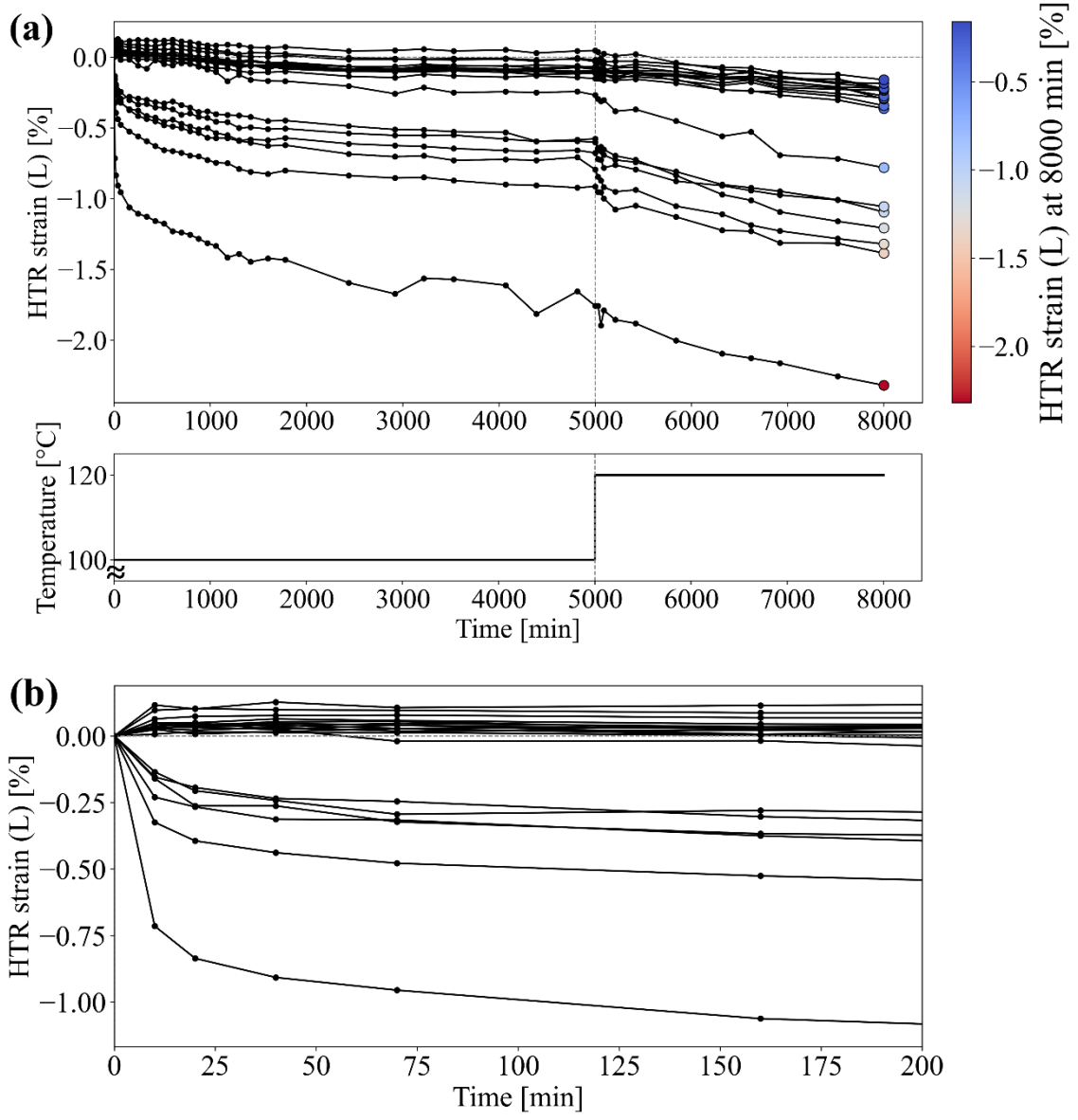

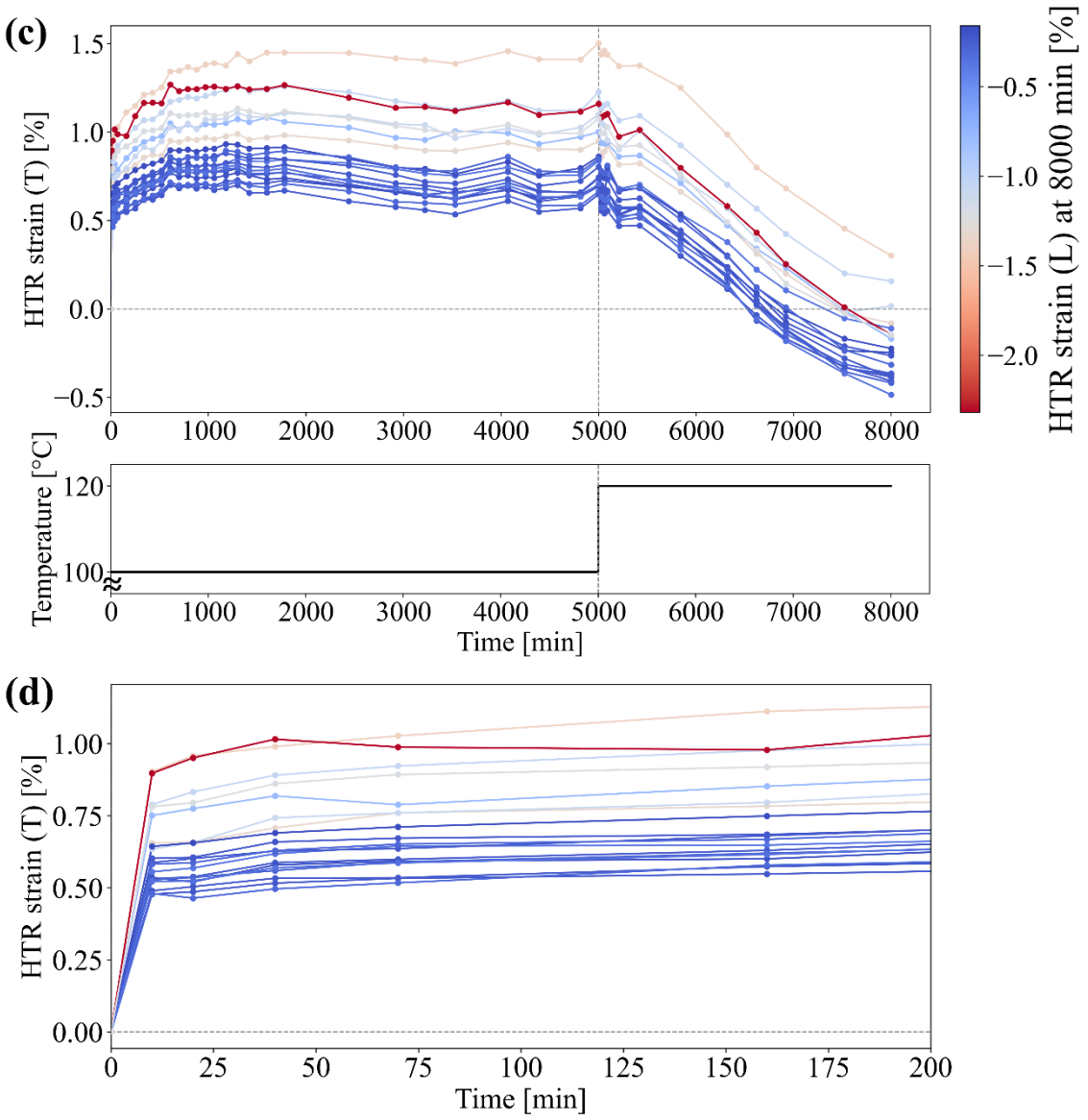

Source: Author's own

Drying mass change

Figure 32 (a)–(d) shows the time dependent evolution of drying mass change from 0 to 4000 min. The drying mass change increased with higher temperatures. Moreover, TW specimens tended to exhibit smaller drying mass change than OW specimens. Figure 32 (e)–(h) show the results from 0 to 200 min. Although, likely Figure 32 (a)–(d), higher temperatures led to larger drying mass change, no clear difference in drying mass change was observed between TW and OW. It was found that the TW shrinks in the L direction and expands in the T direction compared to the OW due to HTR, and this is not because the TW has a higher amount of matrix component elusion.

Figure 32 - Time-dependent evolution of drying mass change to (a)~(d) 4000 min and (e)~(h) 200 min in Group A

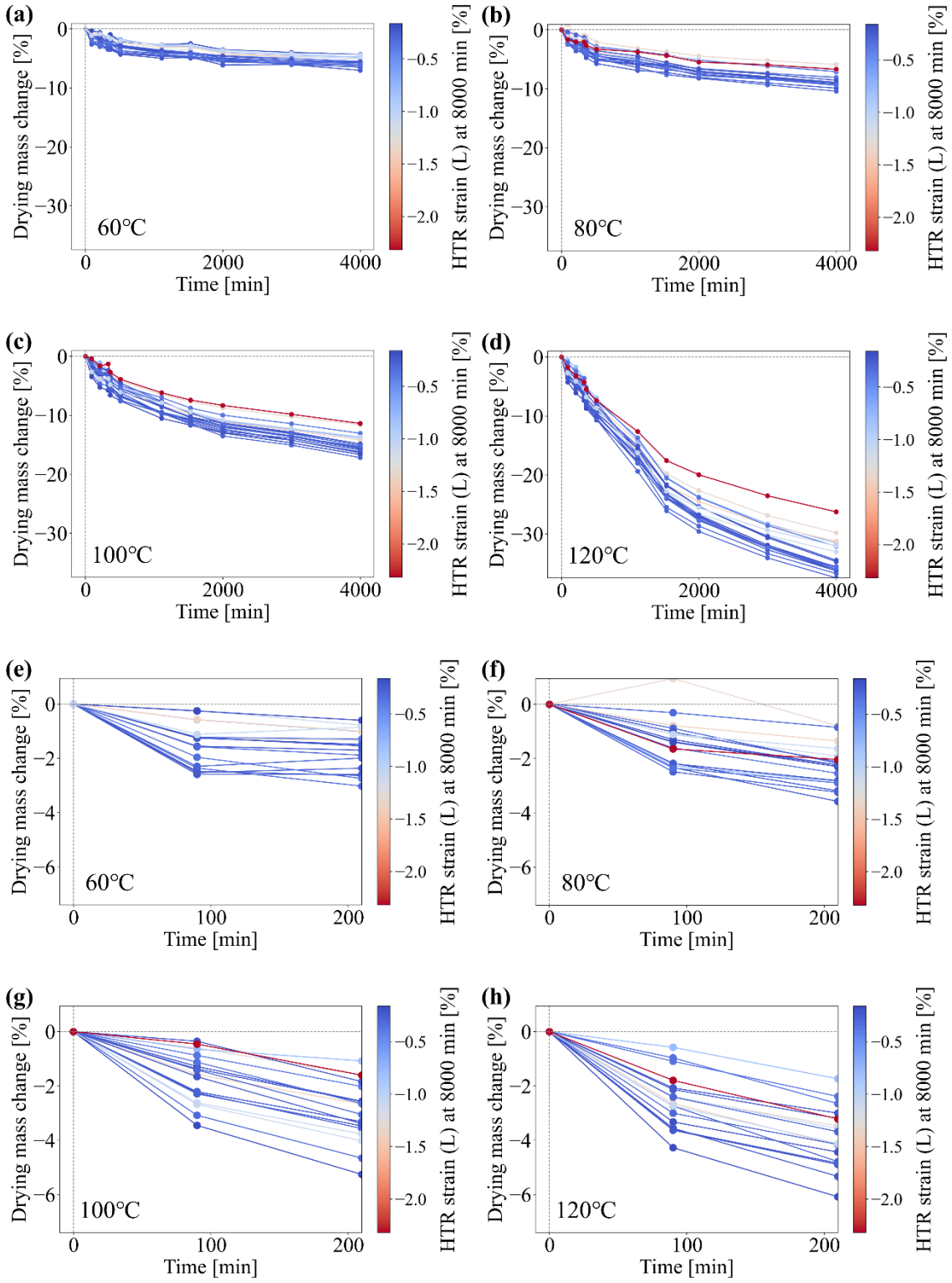

Source: Author's own

4.3.2 HTR strain and *C.I.*, *L* and *d-spacing* of Group B

C.I.

Figure 33 (a)–(d) shows the time-dependent evolution of *C.I.* in Group B during boiling treatment. At the early stage of treatment (0–200 min), *C.I.* decreased once, and thereafter, as the treatment time increased to 2030 and 4000 min, *C.I.* gradually increased. Figure 33 (e) shows the rate of change at each time point, categorized by treatment temperature and by TW or OW. Specimens with *C.I.* at 0 min more than 75% were classified as TW, and those with *C.I.* at 0 min less than 75% were classified as OW. Regarding the decrease in *C.I.* during 0–200 min, OW exhibited a greater decrease rate than TW. For the increase in *C.I.* during 200–2030 min, OW at 100 °C and 120 °C showed larger increase rates. For the increase in *C.I.* during 2030–4000 min, TW tended to show smaller increase rates compared to OW. The decrease or increase in *C.I.* is considered to be influenced by the corresponding changes in I_{amor} due to the thermal motion, decomposition, and leaching of matrix components.

Figure 33 - Time-dependent evolution and change rate of *C.I.* in Group B

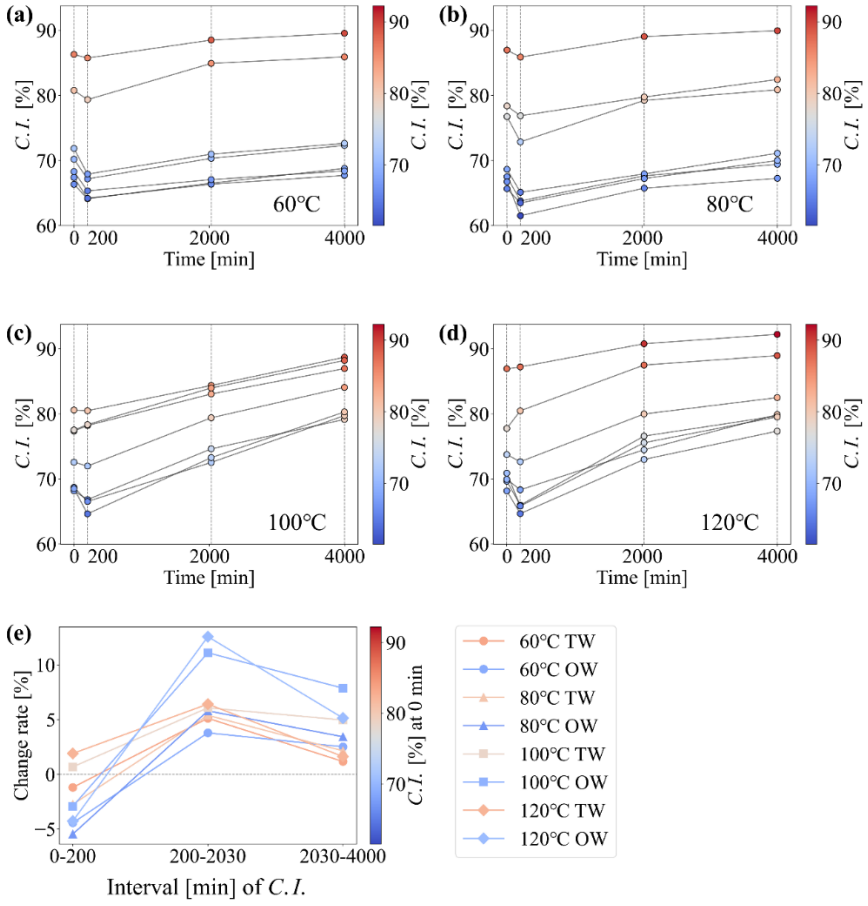

Source: Author's own

HTR strain

Figure 34 (a)–(d) shows the time-dependent evolution of HTR strain (L). The color of the plots at the right edge of each graph indicates the magnitude of *C.I.* at 0 min. Specimens with *C.I.* at 0 min greater than 75% were classified as TW, and those with *C.I.* of 75% or less were classified as OW. TW tended to exhibit larger shrinkage within 0–200 min. At 4000 min, the amount of shrinkage increased with higher treatment temperatures. OW showed almost no dimensional change from 0 to 4000 min at 60 °C, slight shrinkage between 2000 and 4000 min at 80 °C, and gradual shrinkage at 100 °C and 120 °C. The overall trends were consistent with previous studies (e.g. Yamamoto *et al.* 2022). Exceptions included specimens at 100 °C that, despite a large *C.I.* at 0 min, did not show significant shrinkage within 200 min, and specimens at 120 °C that, despite a small *C.I.* at 0 min, did show considerable shrinkage within 200 min.

Figure 34 (e)–(h) show the time-dependent evolution of HTR strain (T). During 0–200 min, TW tended to elongate more than OW. Thereafter, at 4000 min, HTR strain decreased at 120 °C, whereas at other temperatures it remained nearly constant. Like the L direction, the overall trends were consistent with previous studies. Exceptions included specimens at 100 °C that, despite having a large *C.I.* at 0 min, showed only small elongation within 200 min.

The presence of exceptions compared to previous studies is likely since the specimens used for measuring HTR strain and those used for measuring *C.I.* were different, even though they were continuous in the L direction.

From the results in the L- and T-directions, it can be inferred that boiling at 80–100 °C for 200 min can release approximately 70–75% of the strain (compared with that at 4000 min), while boiling at 120 °C for more than 200 min may cause degradation of the matrix (as indicated by the behavior in the T-direction). Therefore, in industrial applications, boiling at 80–100 °C for around 200 min is an effective method for releasing growth stress on a laboratory scale.

Figure 34 - Time-dependent evolution of HTR strain in Group B

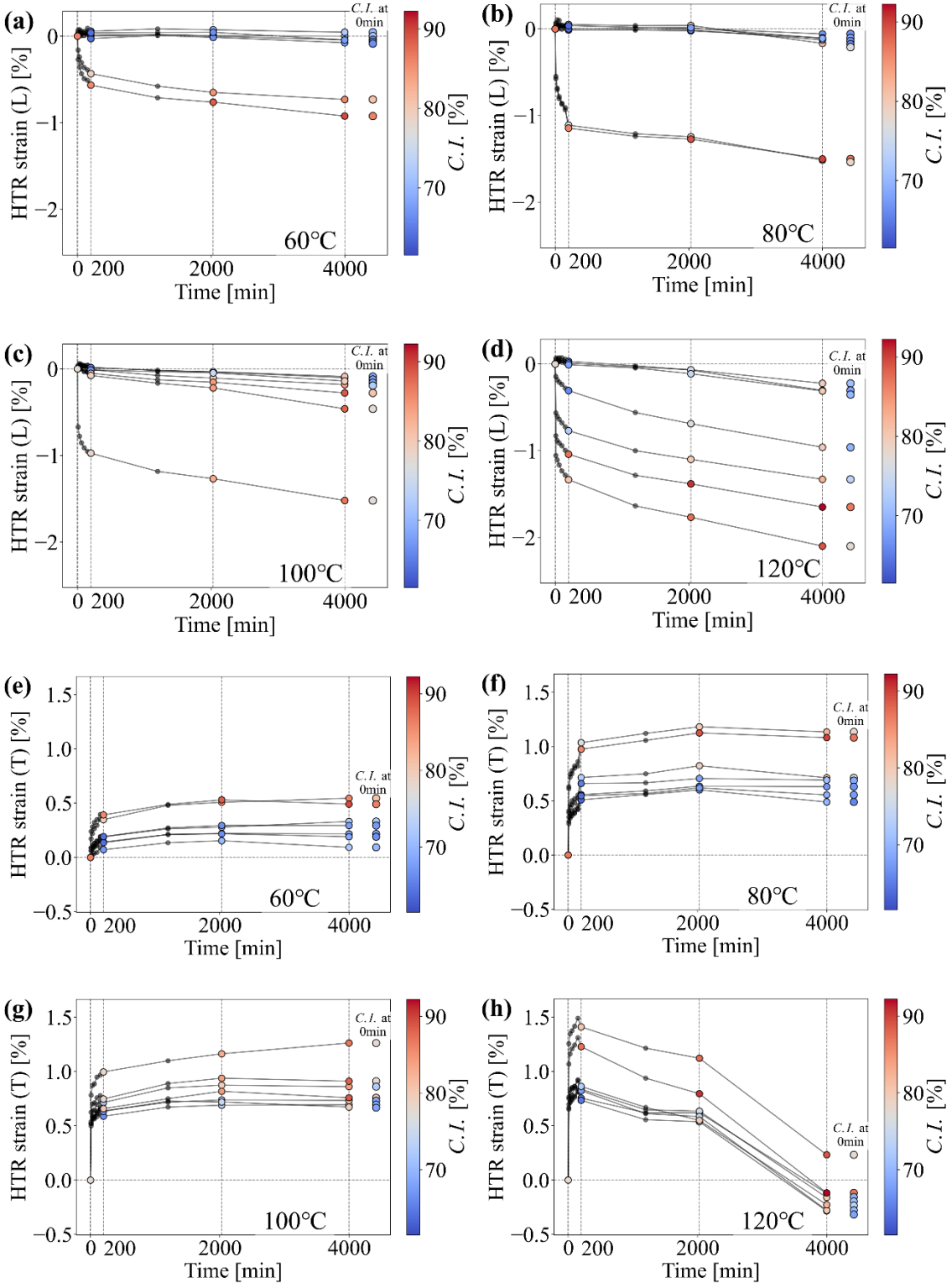

Source: Author's own

The crystallite size (L)

Figure 35 (a)–(d) show the time dependent evolution of crystallite size (*L*) in Group B. An increasing trend was observed from 0 to 200 min after treatment. This result was consistent with (Toba *et al.* 2013a)). Thereafter, the crystallite size increased gradually. Figure 35 (e) presents the rate of change at each time point, categorized by temperature and by TW or OW. Regarding the increase during 0–200 min, TW exhibited a larger increase rate than OW. Furthermore, higher temperatures resulted in larger increase rates. During 200–2030 min, TW and OW at 100 °C and 120 °C showed particularly large increase rates. During 2030–4000 min, OW at 100 °C and 120 °C exhibited especially large increase rates. The increase in crystallite size (*L*) is considered to be due to the development and co-crystallization (Kuribayashi *et al.* 2016) of cellulose crystallites associated with the decomposition and leaching of matrix components, particularly at 100–120 °C.

Figure 35 - Time-dependent evolution and change rate of crystallite size (*L*) in Group B

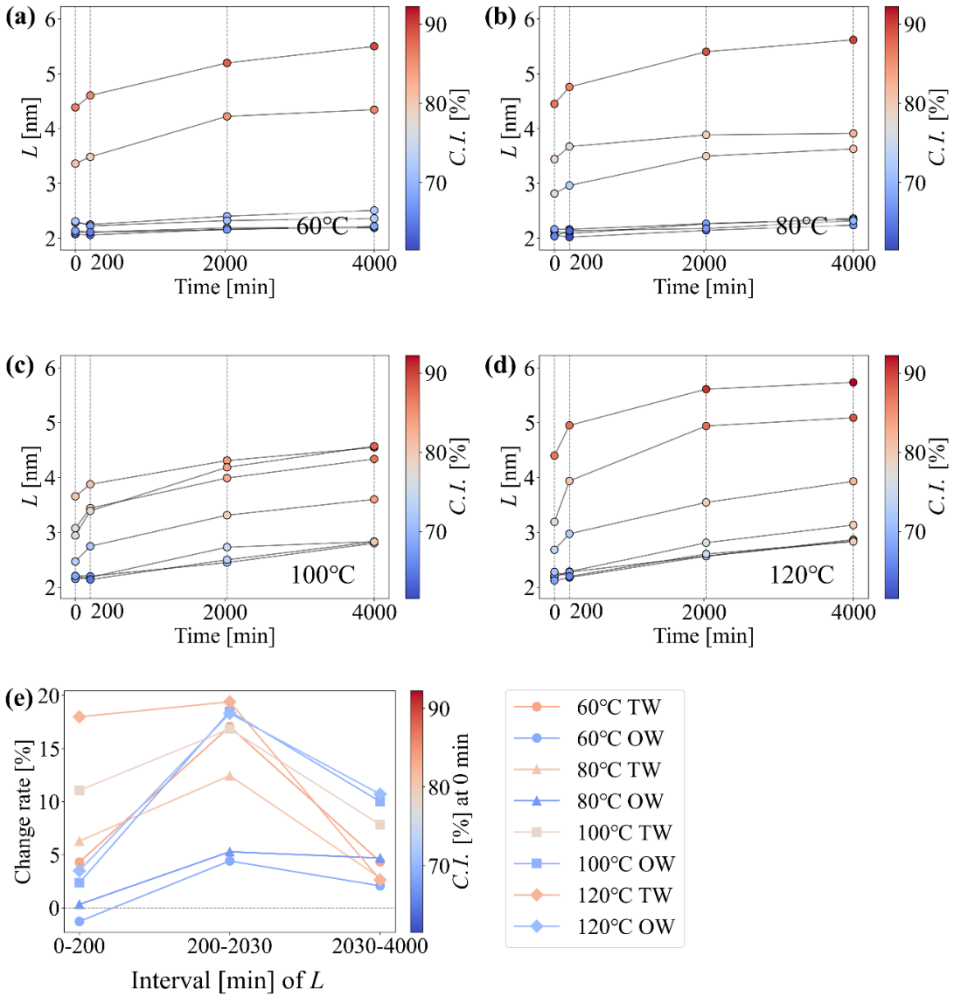

Source: Author's own

D-spacing at (004) plane

Figure 36 (a)–(d) show the time dependent evolution of *d-spacing* at (004) plane in Group B during boiling treatment. No temperature-dependent or TW/OW-dependent trends were observed in the *d-spacing* of surface 004. This result was consistent with Abe and Yamamoto 2007 but not consistent with Toba *et al*. 2013b.

One possible reason for the differing results from previous studies is that irradiating the tangential surface of the test specimen causes the 004 peak to diminish. In this study, irradiation was applied only to the tangential surface to measure the 200 peak simultaneously. Future research should irradiate the end grain surface to investigate the detailed peaks.

Figure 36 - Time-dependent evolution and change rate of *d-spacing* at (004) plane in Group B

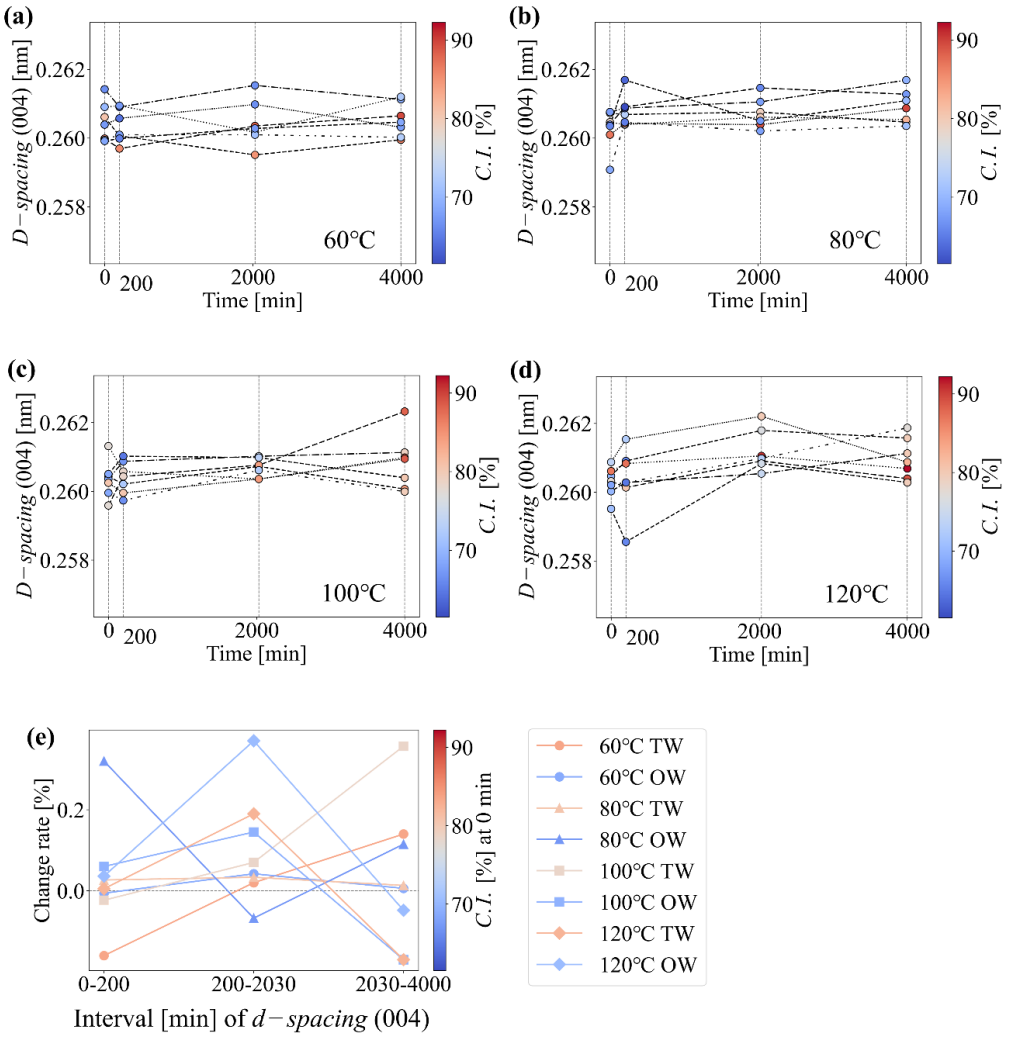

Source: Author's own

D-spacing at (200) plane

Figure 37 (a)–(d) show the time dependent evolution of *d-spacing* at (200) plane in Group B during boiling treatment. An increasing trend of *d-spacing* was observed within 0–200 min after treatment. This result was consistent with (Abe and Yamamoto 2006) and (Toba *et al.* 2013b). Thereafter, a gradual decrease was observed between 200 and 2030 min, followed by either a decrease or stabilization between 2030- and 4000-min. Figure 37 (e) presents the rate of change at each time point, categorized by temperature and by TW or OW. Regarding the increase in 0–200 min, OW exhibited a larger increase rate than TW. For the decreasing trend of *d-spacing* during 200–2030 min, OW showed a greater decrease rate than TW. During 2030–4000 min, TW tended to show smaller decrease rates compared to OW.

The increase in *d-spacing* at (200) plane during 0–200 min is considered to suggest the release of surface growth stress in the T direction (Abe and Yamamoto 2006). Although TW exhibited greater elongation in the T direction by HTR (Figure 34 (e)–(h)), its increase rate of *d-spacing* was smaller than that of OW. This is considered to be due to the presence of the G-layer in TW, which contains abundant cellulose crystallites in the innermost layer of xylem fibers, and the increase in *d-spacing* of these crystallites accumulated in the T direction. The subsequent decrease in *d-spacing* is considered to result from matrix degradation. And this finding is critical for the mechanistic model. The result suggests that the observed total macroscopic T-elongation in TW is a sum of two components: (1) Crystalline Release (measured by d200 expansion), which is less dominant in TW, and (2) G layer/Matrix Relaxation (bulk viscoelastic swelling), which is the dominant contributor to the greater overall macro elongation observed in TW. This result definitively separates the mechanical action of the G-layer from the crystalline core's stress release mechanism.

Figure 37 - Time-dependent evolution and change rate of *d-spacing* at (002) plane in Group B

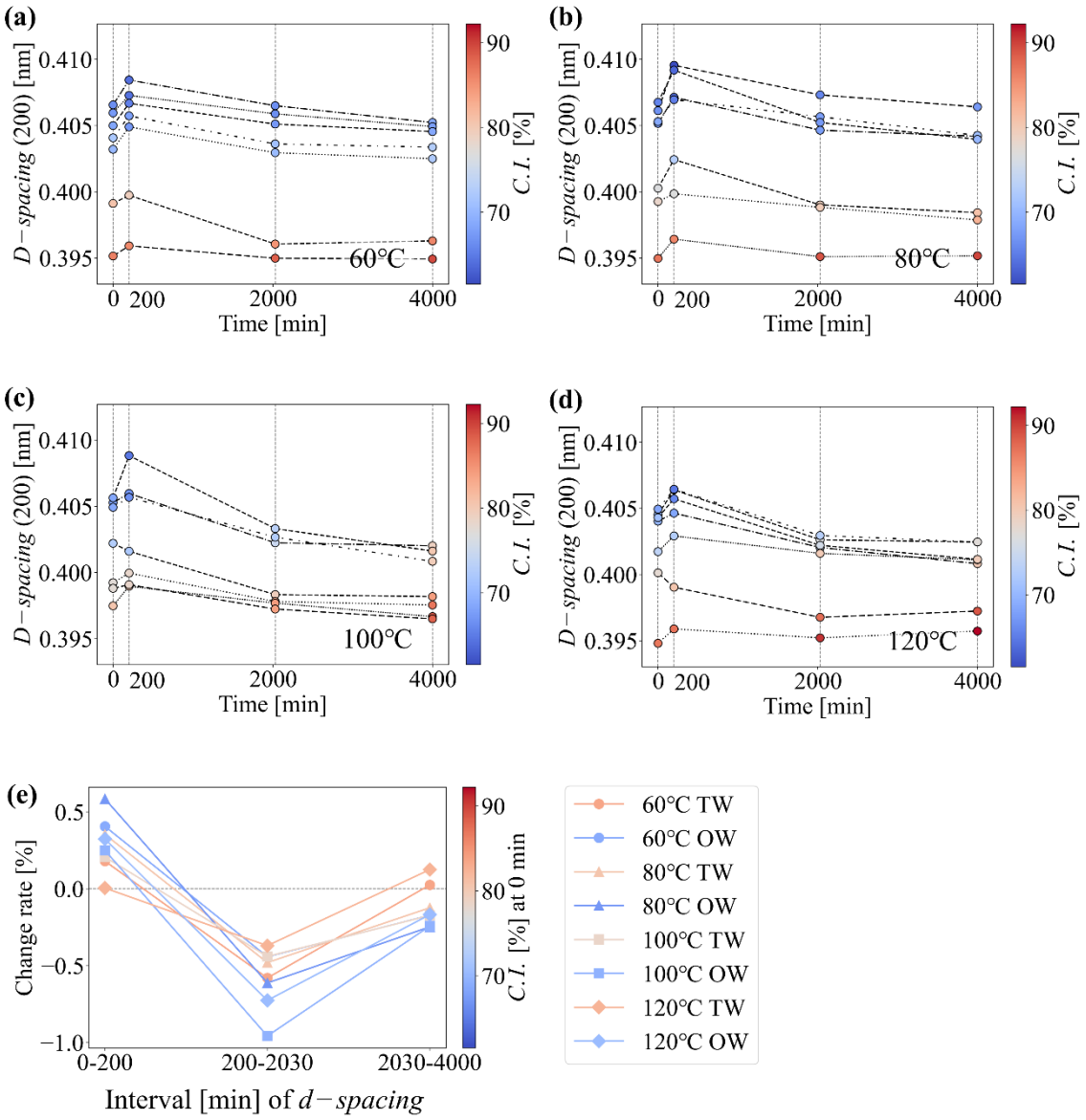

Source: Author's own

4.4 Conclusion

The shrinkage of TW in the L direction and its elongation in the T direction compared to OW, observed through the release of viscoelastic components under growth stress (HTR), was suggested to be influenced not by TW having a higher matrix component elution rate, but rather by differences in matrix composition, ease of matrix degradation and elution, and cellulose crystal development and co-crystallization. Furthermore, it was suggested that in the L direction, structural changes in CMF (such as twisting) at a level beyond the cellulose molecular chain level may be influential, while in the T direction, the expansion of the cellulose molecular chain network may be influential (Figure 38). These factors are considered to be involved in the mechanism of growth stress generation and release.

Figure 38 - The hypothesis of mechanism of growth stress generation and releasing

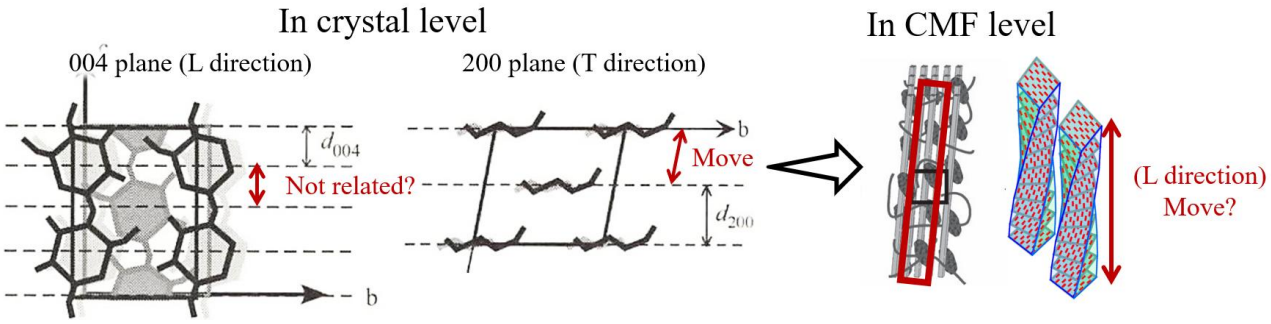

Source: Author's own based on Fernandes *et al.* 2011 and Secondary Xylem Formation 2011.

References

ABE, K.; YAMAMOTO, H. Mechanical interaction between cellulose microfibril and matrix substance in wood cell wall determined by X-ray diffraction. **J Wood Sci**, v. 51, p. 334–338, 2005.

ABE, K.; YAMAMOTO, H. Change in mechanical interaction between cellulose microfibril and matrix substance in wood cell wall induced by hygrothermal treatment. **J Wood Sci**, 52:107–110, 2006.

ABE, K.; YAMAMOTO, H. The influences of boiling and drying treatments on the behaviors of tension wood with gelatinous layers in Zelkova serrata. **J Wood Sci**, v. 53, p. 5–10, 2007.

BARDET, S.; GRIL, J.; KOJIRO, K. Thermal Strain of Green Hinoki Wood: Separating the Hygrothermal Recovery and the Reversible Deformation. In: FRÉMOND, M.; MACERI, F. (eds). **Mechanics, Models and Methods in Civil Engineering**. **Springer Berlin Heidelberg**, Berlin, Heidelberg, pp. 157–162, 2012.

CAPRON, M.; BARDET, S.; SUJAN, K. C.; *et al*. Viscoelastic modeling of wood in the process of formation to clarify the hygrothermal recovery behavior of tension wood. **J Mater Sci**, 53:1487–1496, 2018.

CHEN, S.; MATSUO-UEDA, M.; YOSHIDA, M.; YAMAMOTO, H. Hygrothermal recovery of compression wood in relation to DMSO swelling and drying shrinkage. **Holzforschung**, 74:789–797, 2020.

CHEN, S.; MATSUO-UEDA, M.; YOSHIDA, M.; YAMAMOTO, H. Hygrothermal recovery behavior of cellulose-rich gelatinous layer in tension wood studied by viscoelastic vibration measurement. **Cellulose**, 28:5793–5805, 2021.

FERNANDES, A. N.; THOMAS, L. H.; ALTANER, C. M.; *et al*. Nanostructure of cellulose microfibrils in spruce wood. **Proc Natl Acad Sci USA**, 108: E1195-E1203, 2011.

FOOD AND AGRICULTURE ORGANIZATION OF THE UNITED NATIONS (FAO). Unasylva, Vol. 20 (1-2): An International Review of Forestry and Forest Industries – Wood: World Trends and Prospects. Rome: **FAO**, 1966.

FUKUSHIMA, K.; FUNADA, R.; SUGIYAMA, J.; TAKABE, K.; UMEZAWA, T.; YAMAMOTO, H. (Eds.). **Secondary Xylem Formation - Introduction to Biomass Science (2nd ed.)**. **Kaiseisha Press**, 2011.

GRIL, J.; JULLIEN, D.; BARDET, S.; YAMAMOTO, H. Tree growth stress and related problems. **J Wood Sci**, 63:411–432, 2017.

GRIL, J.; THIBAUT, B. Tree mechanics and wood mechanics: relating hygrothermal recovery of green wood to the maturation process. **Ann For Sci**, 51:329–336, 1994.

KITAHARA, R.; TSUTSUMI, J.; MATSUO, T. Wood Deformations Due to Growth Stress Release. **Bulletin of the Utsunomiya University Forests**, 22:49–60, 1986.

KURIBAYASHI, T.; OGAWA, Y.; ROCHAS, C.; *et al*. Hydrothermal Transformation of Wood Cellulose Crystals into Pseudo-Orthorhombic Structure by Cocrystallization. **ACS Macro Lett**, 5:730–734, 2016.

MATSUO-UEDA, M.; YOSHIDA, M.; YAMAMOTO, H. Analysis of hygrothermal recovery of tension wood induced by boiling at 50–80 °C. **Holzforschung**, 77:270–282, 2023.

OKUYAMA, T.; YAMAMOTO, H.; YOSHIDA, M.; *et al*. Growth stresses in tension wood: role of microfibrils and lignification. **Ann For Sci**, 51:291–300, 1994.

SEGAL, L.; CREELY, J. J.; MARTIN, A. E.; CONRAD, C. M. An Empirical Method for Estimating the Degree of Crystallinity of Native Cellulose Using the X-Ray Diffractometer. **Textile Research Journal**, 29:786–794, 1959.

SUJAN, K. C.; YAMAMOTO, H.; MATSUO, M. U.; *et al*. Delayed recovery of growth stress in tension wood induced by drying and subsequent wetting treatment. **Wood Sci Technol**, 52:1049–1060, 2018.

TANAKA, M.; YAMAMOTO, H.; YOSHIDA, M.; *et al*. Retarded recovery of remaining growth stress in Agathis wood specimen caused by drying and subsequent re-swelling treatments. **Eur J Wood Prod**, 73:289–298, 2015.

TOBA, K.; YAMAMOTO, H.; YOSHIDA, M. On the mechanical interaction between cellulose

microfibrils and matrix substances in wood cell walls: effects of chemical pretreatment and subsequent repeated dry-and-wet treatment. **J Wood Sci**, 59:359–366, 2013a.

TOBA, K.; YAMAMOTO, H.; YOSHIDA, M. Micromechanical detection of growth stress in wood cell wall by wide-angle X-ray diffraction (WAX). **Holzforschung**, 67:315–323, 2013b.

YAMAMOTO, H.; SUJAN, K. C.; MATSUO-UEDA, M.; *et al*. Microscopic mechanism of contraction of tension wood G-fiber due to boiling. **Cellulose**, 29:7935–7954, 2022.

YAMAMOTO, H.; YOSHIDA, M.; OKUYAMA, T. Growth stress controls negative gravitropism in woody plant stems. **Planta**, 216:280–292, 2002.

YOSHIDA, M.; OHTA, H.; OKUYAMA, T. Tensile growth stress and lignin distribution in the cell walls of black locust (Robinia pseudoacacia). **J Wood Sci**, 48:99–105, 2002.

Chapter 5: Final discussion

This study conclusively demonstrates that HTR is the most effective and quantifiable method for releasing the viscoelastic component of growth stress in wood. It provides the foundational data for two key commercial outcomes: (1) Process Optimization: Establishing minimum energy and time requirements for industrial steaming to maximize residual stress relief (at 80 – 100℃ for around 200 min), and (2) Quality Assurance (QA): Validating HTR strain as a powerful, log-specific QA parameter for predicting internal stress profiles before high value sawing process.

In Chapter 3, the results showed that HTR alone exhibited dependence on the distance from the pith and contributed to the release of the viscoelastic component of growth stress. In chapter 4, it was found that the viscoelastic components of growth stress may be released at a more macroscopic level (e.g., CMF) between cellulose molecules in the longitudinal (L) direction, while in the tangential (T) direction, released between cellulose chains.

These findings are considered important for elucidating the mechanisms of growth stress release and generation. Understanding the mechanism of growth stress release could potentially help overcome defects such as warping and cracking during wood utilization, while understanding the mechanism of growth stress generation may enable control over tree form. For future studies, analysis using FTIR and small-angle scattering are desirable to elucidate the behavior of the matrix and CMFs during HTR.

Although research on growth stress is still developing, it is expected to become increasingly important in the context of a sustainable society.